Photogrammetric Deformation Analysis of a Quay Wall

Stochastic non-linear least-squares deformation analysis from photogrammetric measurements of a quay wall

H.C. Lodder

Msc. Thesis

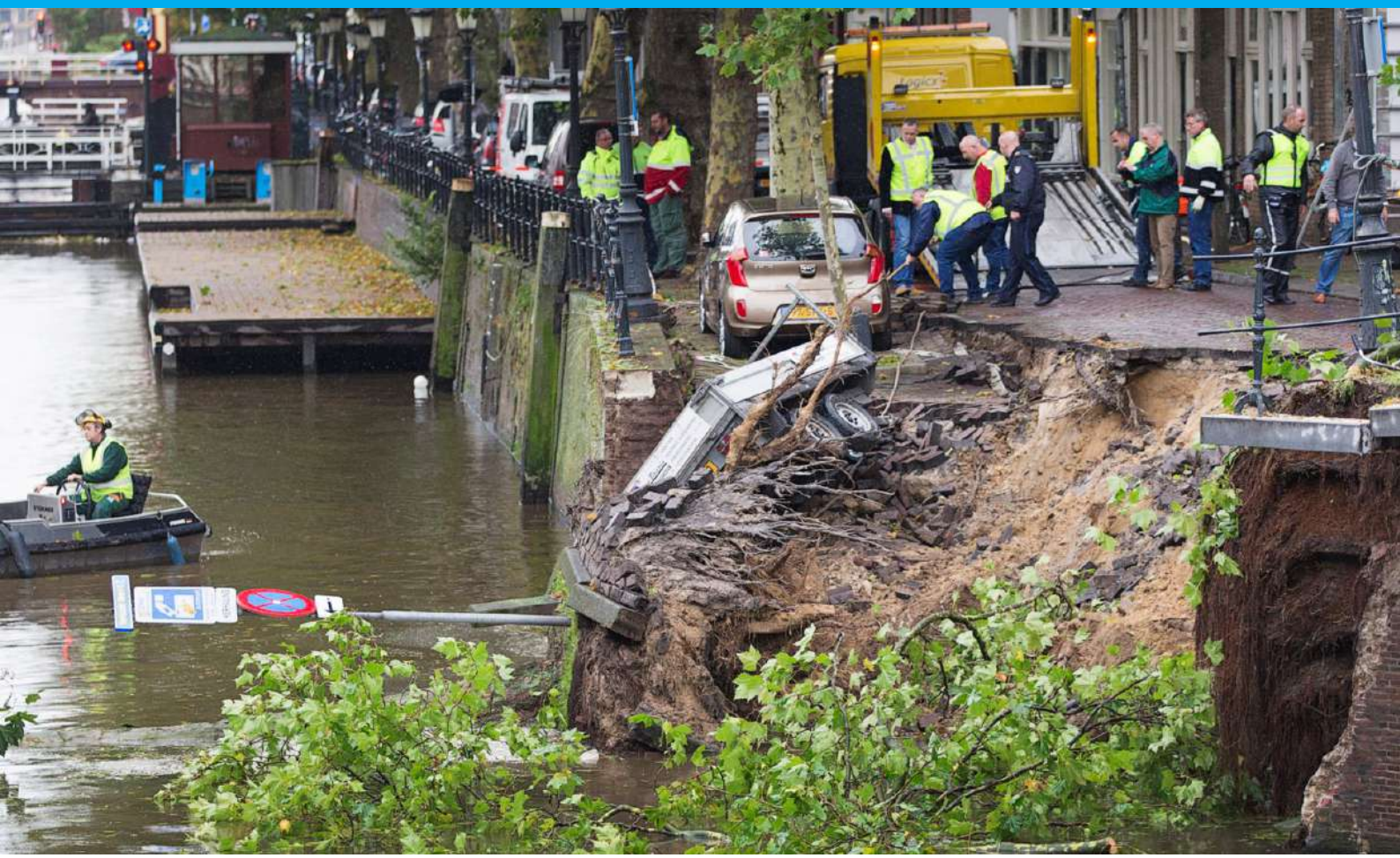

TU Delft Delft University of Technology

GEODELTA

Photogrammetric Deformation Analysis of a Quay Wall

Stochastic non-linear least-squares deformation analysis from photogrammetric measurements of a quay wall

by

H.C. Lodder

to obtain the degree of Master of Science
at the Delft University of Technology,

Student number:	4574621	
Project duration:	February 15, 2021 – October 21, 2021	
Thesis committee:	Dr. R. Lindenbergh,	TU Delft, chair
	Dr. A. Amiri Simkooei	TU Delft
	ir. P.A. Korswagen	TU Delft
	ir. M.P. Kodde,	Geodelta, supervisor

An electronic version of this thesis is available at http://repository.tudelft.nl/.

TU Delft

Abstract

In recent years, unstable quay walls are a problem in The Netherlands. 100-year-old quay walls in cities like Amsterdam are collapsing and endanger people and property. The government needs to renovate unstable quay walls quickly. With 600 kilometre of quay wall in Amsterdam alone, this is a great challenge. Currently, unstable walls are found by deformation monitoring using tacheometry, which takes too much time for large scale monitoring. To increase both speed and coverage, a photogrammetric deformation analysis is proposed. In multiple epochs, at months interval, a series of images of the quay wall is made from a boat. In these images, feature points are identified and matched, where part of the feature points are matched across multiple epochs. All feature point observations are put in a multi-epoch least squares adjustment. This adjustment integrates both feature point observations of individual epochs and point deformations between multiple epochs. Using photogrammetry in combination with such a deformation adjustment has not been done previously, but has great advantages. The least squares adjustment allows to take the stochastic nature of the observations into account. This enables proper error propagation, such that not only quay wall stability can be assessed, but also the corresponding error budget. Results show that using two epochs 300 multi-epoch feature points can be found per square meter quay wall. With these points, sub-centimetre deformation can be estimated.

Contents

1 Introduction

1.1. Collapsing quay walls

In recent years in the Netherlands a problem has arisen. Old quay walls along the canals in the old cities are becoming unstable. This can result in the quay walls collapsing. This recently happened at the Grimburgwal in Amsterdam, where 20 meters of quay wall suddenly collapsed into the canal [25].

Figure 1.1: Collapsed Grimburgwal, Amsterdam [25].

In reaction to the dangers of collapsing quay walls (and bridges), the city of Amsterdam has made plans to renovate the quay walls. However, there are 600 kilometers of quay wall in Amsterdam alone, of which 200 kilometers are already prioritized for renovation. The time estimated to renovate the 200 kilometers of priority quay wall is 20 years at a minimum [10]. And this problem is not specific to Amsterdam. Utrecht, The Hague and other Dutch cities also have many kilometers of quay wall with similar dangers.

The city of Amsterdam has made a plan of what to do with the quay walls [10]. A main point in this plan is to guarantee safety by identifying unstable quay walls and taking precautions. For example by limiting traffic near the quay walls. The deformation is used as an indicator of instability. Deformation monitoring requires much measuring, so much that the city of Amsterdam started a competition for quay wall monitoring innovations [30].

1.2. Monitoring

Currently this monitoring is done by surveyors with tacheometry. They measure the quay wall at different times (epochs) with a couple of months in between. The exact length of the interval is dependent on the expected stability of the wall. The quay wall is measured in on the same set points in every epoch. At these set points on the wall prisms can be installed to make the tacheometric measurements more accurate. When properly used, the tacheometers deliver measurements at millimeter precision [32] [12]. This makes it good for these high precision deformation measurements. However, with a tacheometer not many points are measured on the quay wall, as every point has to be manually measured from multiple positions, which is time consuming. Also, these measured points must be consistent between epochs to get deformation so, there is always risk of losing measurement points.

The use of photogrammetry to monitor the quay walls can solve these problems. Photogrammetry has the potential of making the monitoring of the quay walls more cost and time efficient and more robust with many measurement points on the walls. However, photogrammetric measuring of the quay walls also brings some potential problems. Is it possible to match features in images from different epochs and is it possible to reach high enough accuracy to be able to detect small deformation? These problems have to be explored to assess the extend to which photogrammetric measurements of a quay wall can be used in deformation analysis.

Also, the currently used tacheometric deformation analysis only performs adjustment on the measurements in a single epoch and then the deformation is found by simply calculating the differences in coordinates. This method is flawed as the uncertainty in the measurements, also known as the stochastic characteristics of the measurements, are only taken into account for the single epoch calculations and they are ignored when calculating the deformation. Integrating multiple epochs and the deformation between the epochs in the adjustment allows to use the stochastic characteristics directly in the deformation estimation. This direct use of stochastic measurements for the deformations in turn allows to use statistical testing on the deformation parameters. As the photogrammetric equations are non linear equations the least squares adjustment does require a linearisation.

1.3. Main research question and subquestions

The main research question of this MSc thesis is:
To what extend is it possible to do stochastic least-squares adjustment based deformation analysis on a quay wall using photogrammetry?

Answering this question will lead to subquestions such as:

- What are the requirements from organisations involved?
- What is the data acquisition workflow for photogrammetric deformation analysis?
- How to form observations from the photogrammetric measurements?
- How to build the non-linear stochastic least-squares adjustment for deformation analysis?
- How to test the adjustment to find the best hypothesis?
- What quality of deformation is possible? Is this quality good enough?

2

Monitoring of Quay walls and Photogrammetry

In this chapter findings of a literature research are presented. The research is done in three fields important to this thesis. Research findings in these fields are in turn presented, starting with deformation of quay walls. Then follows the basics of photogrammetry, and finally deformation analysis.

2.1. Quay wall Deformation

2.1.1. Failure mechanisms

To make hypotheses of the deformation that may be found in quay walls, the deformation and failing mechanisms of quay walls are researched. There are multiple types of quay wall. Roubos et al. [27] distinguishes four types.

1. Steel founded gravity wall
2. Pile founded gravity wall
3. Pile founded L-wall
4. Steel or concrete sheet pile wall

The brick quay walls at risk of collapse are type 2, a pile founded gravity wall. The foundation piles of these quay walls are wooden and the quay wall are brickwork and they are old, with many walls exceeding 100 years. Roubos et al. [27] defines eight failure mechanisms relevant to pile founded quay walls. These failure mechanisms are defined by Roubos et al. [27] and they are both geotechnical and structural. The failure mechanisms are listed below in Table 2.1 and shown in Figure 2.1.

1	Exceeding vertical pile compression capacity.
2	Exceeding vertical pile tension capacity.
3	Exceeding horizontal pile loading capacity.
4	Exceeding general stability.
5	Structural failure quay wall.
6	Structural failure of foundation piles.
7	Foundation pile failure from displacement.
8	Erosion by underground water flow.

Table 2.1: List of Quay wall failure mechanisms as defined by Roubos et al. [27].

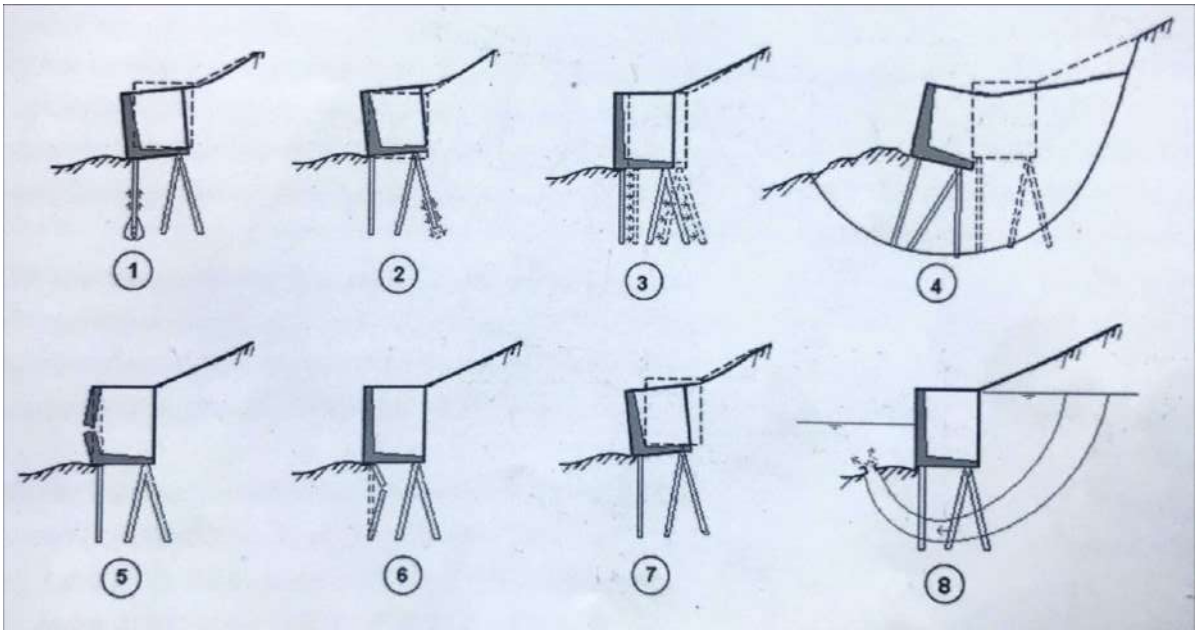

Figure 2.1: Failure mechanisms of a pile founded quay wall as defined by Roubos et al. [27], visualized where the number corresponds to the failure mechanis in Table 2.1.

An interesting case of collapsing quay wall is the collapse of the Grimburgwal on September first 2020. This collapse is investigated and a rapid assessment is already published [17]. The collapse of the Grimburgwal is suspected to be caused by failure of the wooden foundation piles from horizontal deformation, which would be a combination of failure mechanisms 3 and 6 in Figure 2.1. It is found that boats turning at this part of the Grimburgwal creates in a deep canal bed at the quay wall, which was unstable and lead to the horizontal deformation of the quay wall [17]. At the Grimburgwal, there was no sign of deterioration of the wooden piles, however there is suspected pile deterioration in these old quay walls. This is due to a changing water level making the wooden piles dry at times, which could result in the wood rotting.

Korff et al. [17] states that one indicator of coming failure is the horizontal deformation of the quay wall. Pictures of the Grimburgwal from February 2020, seven months before collapse, showed this deformation at street level. Where the horizontal deformation was big enough to create gaps in the streetwork. In addition to deformation, there was damage on the Grimburgwall, which could also be a indication of coming failure.

All failure mechanisms are detectable by a deformation, however it is not possible to determine the type of failure from the deformation alone [33]. All deformations shown are either vertical or horizontally perpendicular to the quay wall. There is no indicated deformation parallel to the quay wall. However, stresses on the quay wall are not homogeneous along the whole quay wall, so there must be change in deformation along the quay wall. Also a failing pile will create a local deformation, which is not homogeneous along the quay wall. At stress locations, where a load on the quay wall is present, and at pile failing locations, the deformation is probably biggest and moving away along the quay wall from that point the deformation probably reduces.

2.2. Photogrammetry

Photogrammetry is the science of obtaining information from images. In present times it is often taken to be a method to extract three dimensional coordinates from multiple two dimensional images. Photogrammetric calculations are based on establishing the geometric relation between the 3D coordinate and the images capturing that coordinate.

2.2.1. Camera

Photogrammetry starts with the camera. In the simplest form a camera is a dark room with a small hole. This is also known as a camera obscura, where the hole is called the the optical center. Light reflects from objects in front of the hole. This light goes through the hole and lands on the wall opposite of the hole. This simple camera is called a pinhole camera and it gives a good view of the geometry of a picture. This basic idea of a camera is already hundreds of years old as can be seen from the Figure 2.2, which is a drawing from Ayscough [2] from 1752.

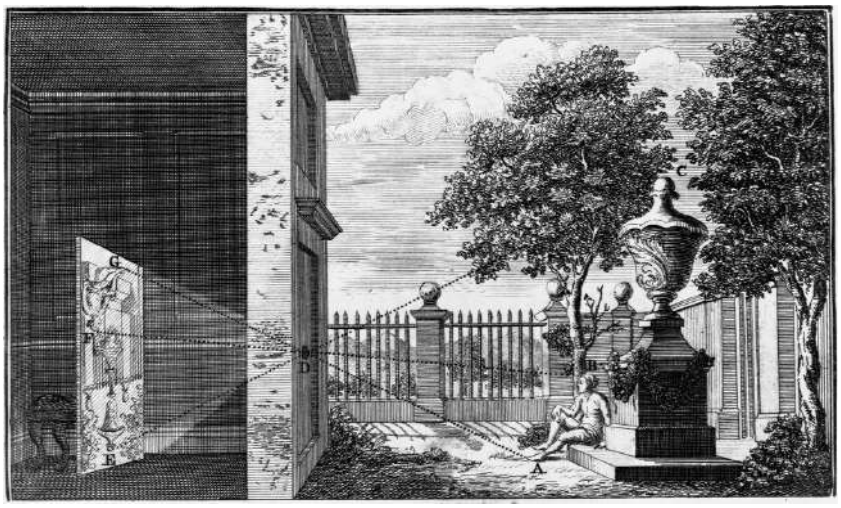

Figure 2.2: Camera obscura as drawn by Ayscough [2], where light passes through a small hole in a dark room projecting an image on the wall opposite the hole.

The light reflected from a object can only move in a straight line through the optical center. This results in a projection of the object on the opposite wall. The opposite wall is the negative image plane and the projection on this plane is mirrored and upside-down. To make it easier to understand the geometries, the positive image plane can also be used. The positive image plane is a imaginary image plane at the same distance from the optical center as the negative image plane, but the positive image plane is between the object and the optical center, which makes for a virtual projection that is not mirrored nor upside-down. This is why in most figures the positive image plane is drawn. The distance from the image plane to the hole is called the focal distance or camera constant.

2.2.2. Collinearity condition

The fact that light goes in a straight line is the principle on which the photogrammetry is build. The straight line makes it that an object point, the optical center and the projection of that object point are on the same line. In photogrammetry this is called the collinearity condition. It leads to geometrical equations that mathematically link the 3D object point coordinate to the 2D image coordinate of the projection of that same object point. These equations are called the collinearity equations and can be seen in Equation 2.1 and Equation 2.2. The collinearity geometry is shown in Figure 2.3. Here, optical center C (X_C, Y_C, Z_C), object point A (X_A, Y_A, Z_A) and the projection of point $A(x_a, y_a)$ on the positive image plane are all on one line.

$$x_a = x_O - f\frac{r_{11}(X_A - X_C) + r_{12}(Y_A - Y_C) + r_{13}(Z_A - Z_C)}{r_{31}(X_A - X_C) + r_{32}(Y_A - Y_C) + r_{33}(Z_A - Z_C)} \tag{2.1}$$

$$y_a = y_O - f\frac{r_{21}(X_A - X_C) + r_{22}(Y_A - Y_C) + r_{23}(Z_A - Z_C)}{r_{31}(X_A - X_C) + r_{32}(Y_A - Y_C) + r_{33}(Z_A - Z_C)} \tag{2.2}$$

where:

x_a, y_a = image coordinates of image point
x_0, y_0 = image coordinates of principal point
X_A, Y_A, Z_A = terrain coordinates of terrain point
X_C, Y_C, Z_C = coordinates of optical center
r_{ii} = elements of the rotation matrix from the orientation of the camera

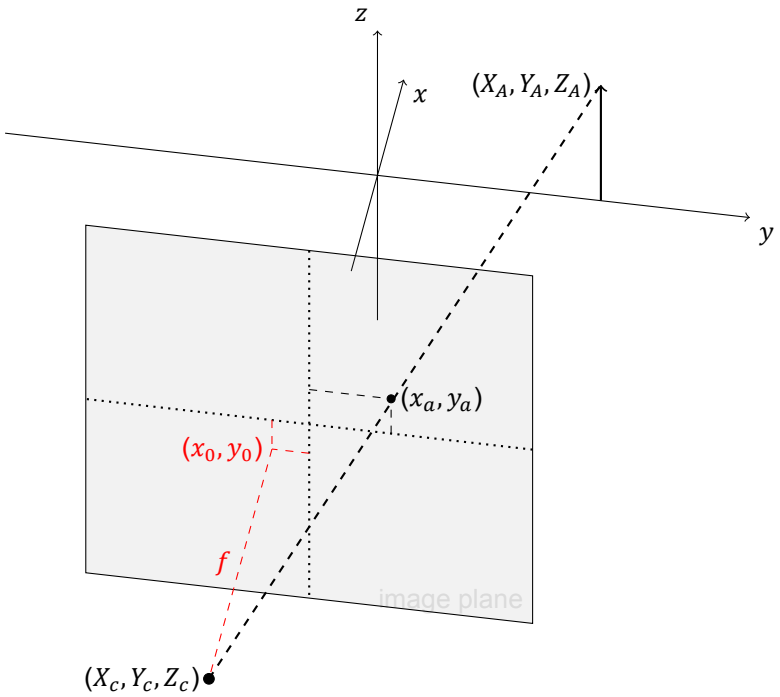

Figure 2.3: Visual representation of the collinearity condition. Point A with coordinates (X_A, Y_A, Z_A) is captured by camera C with optical center coordinates (X_C, Y_C, Z_C). The line between the optical center of camera C and point A crosses the image plane at point a with image coordinates (x_a, y_a). This results Point A, Optical center C and image point a being collinear, meaning they are on one line. The position and orientation of the image plane is determined by the focal distance f, the principal point with coordinates (x_0, y_0) and the orientation of the camera which is the orientation of the line optical center to the image plane center.

There are two coordinate systems present in the collinearity equations, the image coordinate system and the real world (terrain) coordinate system. The image coordinate system, denoted by the lower-case x and y, is a 2D coordinate system on the image plane with the origin in the center of the image plane. The terrain coordinate system, denoted by the upper-case X, Y and Z, is a 3D terrain coordinate system. This can be any cartesian system or local system.

In Figure 2.3 the line from optical center C to terrain point A intersects the image plane (and thus image coordinate system) at image point a. From the position and orientation of the image coordinate system in the terrain coordinate system the position of this image point a can be calculated. That calculation is done with the collinearity equations.

2.2.3. Extrinsics and Intrinsics

Every image coordinate system is located in the terrain coordinate system and can be placed by the position, orientation, focal length and principal point of the camera to which the image coordinate system belongs.

The position (optical center) and orientation of the camera are together known as the exterior parameters or extrinsics. The orientation of the camera is often described in the form of a 3-by-3 rotation

matrix, however it can also be described by Euler angles or a quaternion.

The focal length and principal point are known as the interior parameters or intrinsics of the camera. The principal point is the offset between the origin of the image coordinate system and the perpendicular point from optical center to image plane. Ideally the principal point is (0,0), however cameras are not perfect. The focal length is the distance between image plane and optical center. This depends on the lens of the camera. Most modern lenses are able to change the focal distance, this makes the camera zoom in or out. In photogrammetry the focal distance should be stable, because otherwise the internal geometry changes.

When calibrating the camera these intrinsics can be calculated along with the lens distortion parameters. Modern cameras, contrary to the pinhole camera, have lenses which bring some distortion to the projection by bending the light. This distortion is modelled and can also be viewed as part of the intrinsics. In the calibration procedure a controlled environment is captured by a camera. Where object points are can be very accurately found in the images. For example, chess board square corners or round barcodes, which can be accurately pinpointed by computer vision algorithms. Then photogrammetry is used on the image set and because the objects in the images are controlled and accurate, the intrinsics can be accurately estimated.

Brown distortion lens model

A common lens distortion model comes from Brown [5] [11]. This model can be used with only radial lens distortion or with an extension to include tangential lens distortion. This tangential distortion is also known as lens decentering. In Figure 2.4 a schematic overview of the effect of the distortion types on the ideally rectangular image plane is shown.

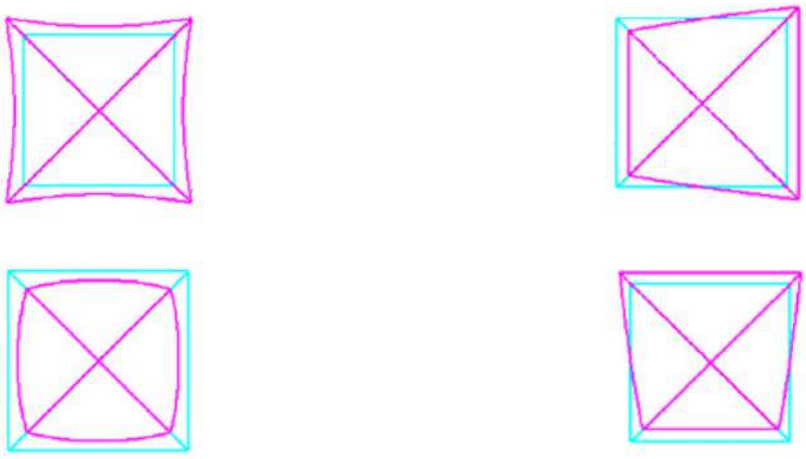

(a) Radial lens distortion

(b) decentering lens distortion

Figure 2.4: Schematic representation of the radial and decentering lens distortion effect on image plane [35]. Light blue is the ideal image plane without distortions and pink is the distorted image plane. For both purely radial and purely decentered distortion two examples are shown.

Radial distortion is modelled using Equation 2.3.

$$dr = A_1 r^3 + A_2 r^5 + A_3 r^7 + ... \tag{2.3}$$

where:

Δr = Radial lens distortion
A_i = Radial distortion constants
r = Radial distance to the principal point

Using Equations 2.4 and 2.5, the Equation 2.3 can be rewritten to get the distortion on the image in x and y direction.

$$\delta x_r = \frac{x}{r} dr \tag{2.4}$$

$$\delta y_r = \frac{y}{r} dr \tag{2.5}$$

where:

δx_r = radial distortion in x direction
δy_r = radial distortion in y direction
x = x-coordinate
y = y-coordinate
r = Radial distance
dr = Radial distortion model

The Tangential distortion is modelled using Equation 2.6 and Equation 2.7.

$$\delta x_t = P_1(r^2 + 2x^2) + 2P_2xy \tag{2.6}$$

$$\delta y_t = P_2(r^2 + 2y^2) + 2P_1xy \tag{2.7}$$

where:

δx_t = tangential distortion in x direction
δy_t = tangential distortion in y direction
P_i = Tangential distortion Constants
x = x-coordinate
y = y-coordinate
r = Radial distance

Combining the radial distortion model and the tangential distortion gives the total distortion as seen in Equation 2.8 and Equation 2.9.

$$\Delta x = \delta x_r + \delta x_t = P_1(r^2 + 2x^2) + 2P_2xy + x * (A_1r^2 + A_2r^4 + A_3r^6 + ...) \tag{2.8}$$

$$\Delta y = \delta y_r + \delta y_t = P_2(r^2 + 2y^2) + 2P_1xy + y * (A_1r^2 + A_2r^4 + A_3r^6 + ...) \tag{2.9}$$

Δx = distortion in x direction
Δy = distortion in y direction
δx_t = tangential distortion in x direction
δy_t = tangential distortion in y direction
δx_r = radial distortion in x direction
δy_r = radial distortion in y direction
P_i = Tangential distortion Constants
A_i = Radial distortion Constants
x = x-coordinate
y = y-coordinate
r = Radial distance

2.2.4. Forward Intersection

The goal of photogrammetry is often retrieval of the 3D position of object points from an image set. Forward intersection is the calculation of a 3D terrain point using its projection in images. For this calculation the collinearity condition is used. It is a geometrical problem, which can be seen in Figure 2.5. For both cameras the projected object point and optical center define a line in 3D space. For each line of a camera the collinearity condition tells us the 3D object point is on that line. With one line and thus one image the 3D position of the object point cannot be estimated as there is no way to tell where on the line the 3D object is. With two images and thus two non-parallel lines this can be done, because

for both these lines it is known that the 3D point is on there the only place where this would be true for both lines is the intersection point. So this intersection point is the 3D object point position.

This problem can also be put as a system of collinearity equations. Trying to calculate a 3D position from a single image results in an under-determined system, because from an image point there are two known variables (image coordinate x and y) and the 3D position has three unknowns (terrain coordinate X,Y and Z). As said above, this can be solved by using more pictures with observations of the same object point. Then more collinearity equations can be made, which increases the amount of known variables while not changing the amount of unknown variables. With two images, both with an observation of the object point, four equations can be formed, which is enough to solve for the 3D terrain point.

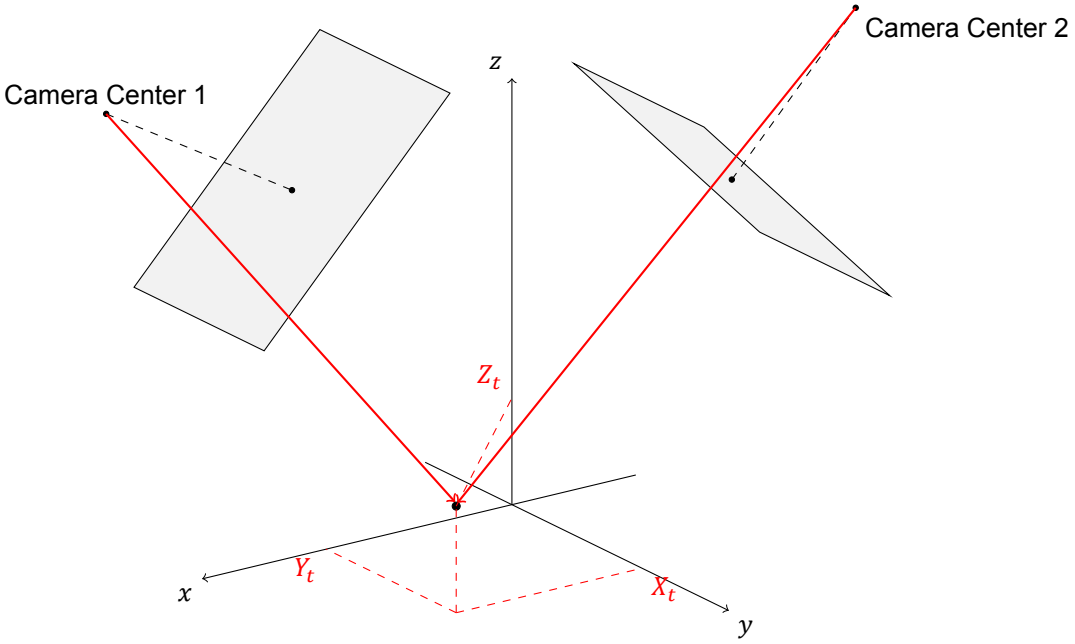

Figure 2.5: Visual representation of the geometry of the forward intersection. Camera 1 and 2 capture point t on their imageplanes a line can be drawn from the camera center through the image point. On this line, the red arrow in the figure, the point must be located in 3D space. As the point t must be on both lines, it can be deduced that the 3D position of point t is on the intersection of the lines.

2.2.5. Backward Intersection

In subsection 2.2.4, the forward intersection estimation uses the assumption that the camera's exterior parameters are known. This can be true, in aerial photogrammetry position and orientation of the camera are often known (approximately) by INS- and GNSS-systems aboard the plane. However, for many cases of photogrammetry the exterior parameters are not known. With backward intersection, also known as resection, the camera exterior parameters can be calculated using known terrain points. The camera exterior parameters are six independent variables. Three for position X, Y, Z and three for rotation *yaw*, *pitch*, *roll*. As said before, rotation can be described in different forms. This does not change the amount of independent variables. With six variables that need to be calculated there would be a need for three terrain points as every terrain point gives two collinearity equations. However, there is an ambiguity to the solution of the backward intersection. This ambiguity comes from the geometric possibility to capture the three points in the same positions with a rotated camera on the other side of the plane through the three points. To solve this ambiguity an extra terrain point is needed. So, in total with four known terrain points in an image the camera exterior parameters can be calculated.

2.2.6. Network Adjustment

Forward and Backward intersection can be expanded using network adjustment methods like Bundle-Block adjustment, where big overdetermined systems are made with many cameras and many object

points. This makes it possible to optimize the calculations and improve the results. As the collinearity equations 2.1 & 2.2 are not linear equations, there is a linearisation of the equations needed in the adjustment.

2.2.7. Object point detection

In all these photogrammetric operations the image points of a terrain point are known to be of the same terrain point in many images. This matching is can be done manually. Look for the terrain point in the images and select where they are. This takes a lot of time and manual labor, so there is need to automate picking object points and matching them between multiple images. There are several algorithms for image feature detection/description and feature matching. The algorithms explained below, SIFT, SURF and ORB are commonly used ones. They are also integrated in OpenCV modules for most coding languages [23].

Using photogrammetry with images taken at different times does add an extra requirement that feature points must be detectable in different conditions, as the conditions can be different between image acquisitions. Environments change and factors like illumination and camera settings are different. The algorithm used for deformation analysis should be able to operate despite these condition changes.

SIFT

SIFT, short for Scale Invariant Feature Transform, is developed by Lowe [19]. SIFT was a big step in finding and describing distinctive features in images. A big advantage to SIFT is the invariance to scale, rotation and translation. Also, there is partial invariance to illumination and affine projection [20]. This is the reason that SIFT is often used. The invariances combined with the distinctive well-described features makes it suitable for photogrammetry. SIFT works in four steps [20]:

1. Scale space extrema detection
2. Keypoint localization
3. Orientation assignment
4. Keypoint Descriptor

First, in the Scale space extrema detection the image is searched for potential features invariant to scale and orientation. This is done by using a difference-of-Gaussian function (DoG) [20]. DoG is an approximation of the Laplacian of Gaussian (LoG). The LoG and DoG are both using Gaussian blurred images and downscaling to make a scale invariant feature detection. However, the LoG uses second order derivatives (Laplacian) and the DoG uses a simple subtraction. As a result the DoG is a faster process, however there is a slight loss in precision [9]. Second, in Keypoint localization, the potential features are fitted to a model to determine location and scale. The keypoints are also evaluated on stability [20]. Third, in Orientation assignment, each keypoint is assigned an orientation based on local image gradients. This is added to the location/scale model of the feature. Future operations on these keypoints can use the orientation/location/scale model to make the features invariant to these transformations [20]. Finally, in Keypoint Descriptor, a description of each keypoint is formed to make a feature. The description uses local image gradients at an selected scale, which makes it resilient to shape distortion and change in illumination [20].

Matching the features between images is the next challenge. SIFT creates many features in an image which can all be linked to features from other images. This is simply done by picking the closest point in an Euclidean space in which the features are positioned according to their feature description vectors [20]. The problem with this approach is that there will be many features, which do not occur in any other image, however it will be assigned to the closest feature resulting in many incorrect matches [20]. This can be solved with a maximum distance threshold to matching.

SURF

An alternative to the SIFT algorithm is the SURF (speed up robust feature) algorithm. Bay et al. [4] propose SURF as algorithm based on similar properties as SIFT, but with lower complexity and better accuracy. The similar properties can also be seen by similar steps in the processing. The difference between SIFT and SURF is mainly in the first step of SIFT. Where SIFT uses the Gaussian blurring

to find potential features, SURF uses the Fast-Hessian Detector based on the Hessian matrix, which is faster in computation than SIFT's Difference-of-Gaussian. The reason for the speed improvement is the use of integral images and box filters [4]. Another difference with SIFT is the descriptor. SURF uses a distribution of Haar-wavelet responses near the feature point as descriptor [4].

ORB
ORB is a newer image feature detection and matching algorithm. It should be two orders of magnitude faster than SIFT according to the developers Rublee et al. [28]. ORB has a different approach to SIFT and SURF for both detection and description of features/keypoints. ORB uses the oriented FAST (oFAST) keypoint detector and rotated-aware BRIEF (rBRIEF) descriptor [28].

FAST [26], a quick corner detection algorithm, is the bases of oFAST. oFAST has some additional processing steps, compared to FAST, to make its functionality in ORB possible [28]. A Harris corner filter [13] is added to reject features on edges. And then FAST plus Harris corner filter is used on multiple scaled versions of the image to account for scaling [16]. FAST does not include an orientation to the feature, which is needed. So, the intensity centroid (IC) technique of Ke and Sukthankar [15] is used to retrieve a orientation.

Then the features are described by rBRIEF. rBRIEF has some additions to the BRIEF [6] keypoint descriptor. In BRIEF n binary intensity tests on smoothed images are used to describe a keypoint in a bit string. BRIEF provides good invariance to lighting, blur and perspective distortion, but is sensitive to in-plane rotation [28]. This rotation sensitivity is solved by steering the BRIEF descriptor using the rotation retrieved in oFAST. Finally, because of the steering of BRIEF and the correlation between binary tests, a greedy search algorithm is used to find the best tests to use in the descriptor. This final descriptor is the rBRIEF, which can be used for image matching by Nearest Neighbour like SIFT and SURF.

2.2.8. Other Feature Matching algorithms
There are also feature matching algorithms in development or recently developed that use deep learning and neural networks. For example, Super Glue [29], which uses a graph neural network. According to Chen et al. [7] the deep learning methods will improve image feature matching. However, they also mention that there is a disadvantage. Deep learning creates black box operations without proper checks. For the development of the photogrammetric quay wall deformation analysis, it is important to have a clear view of the process and its intermediate steps, this is difficult with black box operations. That is why these methods are not chosen to be used.

2.3. Deformation
To measure deformation, measurements in multiple epochs have to be done followed by a time-series analysis used to estimate changes through time, which is the deformation. Velsink [34] proposes a deformation analysis, which resolves three common flaws of other deformation estimations. Firstly, it takes into account the stochastic nature of measurements. Secondly, deformations are mathematically build in the hypotheses and their quality can be statistically tested and evaluated using the observations directly. Finally, statistical analysis of the adjustment used in the deformation analysis can be used to find the best deformation hypothesis.

Velsink [34] both discusses a geodetic observation-based and a coordinate-based analysis. The observation based analysis is better, because there are no intermediate steps where errors can be introduced. Examples of such errors are in calculations of intermediate coordinates and conversion of geodetic datums. In the method of Velsink [34], calculations are directly related to the observations and the stochastic nature of the observations can be directly used. The application of this deformation analysis methodology to photogrammetry is not mentioned by Velsink [34].

2.3.1. Adjustment
The first step in the deformation analysis is the adjustment of the observations. The adjustment model is shown in Equation 2.10 as a matrix equation.

$$\begin{pmatrix} \underline{y}_S \\ z_d \\ z_g \end{pmatrix} = \begin{pmatrix} A_S & 0 \\ Z_d & Z_\nabla \\ Z_g & 0 \end{pmatrix} \begin{pmatrix} x_S \\ x_d \\ x_n \\ \nabla \end{pmatrix} + \begin{pmatrix} \underline{e}_S \\ 0 \\ 0 \end{pmatrix} \tag{2.10}$$

where:

$\underline{y}_S$ = stochastic observation, S indicates epoch number
z_d = nonstochastic observation, constraint linking points between epoch
z_g = nonstochastic observation, constraint determining datum
A_s = observation design matrix
Z_d = epoch linking constraint matrix
Z_g = datum constraint matrix
Z_∇ = deformation matrix
x_S = paramete from observations equations of $\underline{y}_S$, S indicates epoch number
x_d = deformation parameters
x_n = transformation parameters
∇ = deformation model parameters
$\underline{e}_S$ = measurement noise of stochastic observations

And

$$D\{\underline{y}\} = \sigma^2 Q_y = \sigma^2 \begin{pmatrix} Q_{y_S} & 0 & 0 \\ 0 & 0 & 0 \\ 0 & 0 & 0 \end{pmatrix} \tag{2.11}$$

where:

σ^2 = variance of $\underline{y}_S$
Q_{y_S} = observation covariance matrix

Velsink [34] distinguishes three types of observations. The first type of observation is the stochastic observation denoted by $\underline{y}_S$. For photogrammetric applications, these are the observations of the object points in the images. The other two observation types are constraints, which are enforced as non-stochastic observations. Nonstochastic observations z_d set the link between points of different epochs and their movement (deformation) between epochs. Nonstochastic observations z_g set the geodetic datum. These observations make a reference needed to fix the position and orientation of the system in 3D space.

Equation 2.10 can be rewritten to Equation 2.12. Here, Matrix C describes the deformation hypothesis.

$$\underline{y} = A' x_s + C\nabla + \underline{e} = \begin{pmatrix} A' & C \end{pmatrix} \begin{pmatrix} x_s \\ \nabla \end{pmatrix} + \underline{e} \tag{2.12}$$

where:

$\underline{y} = \begin{pmatrix} \underline{y}_s & z_d & z_g \end{pmatrix}^T$
$A' = \begin{pmatrix} A_s & Z_d & Z_g \end{pmatrix}^T$
$C = \begin{pmatrix} 0 & Z_\nabla & 0 \end{pmatrix}^T$
$x_s = \begin{pmatrix} x_c & x_d & x_n \end{pmatrix}^T$

Transformation in adjustment

In the deformation analysis of Velsink [34] the change in shape of the system is the deformation. Meaning a change in relative distances between points in the system. To do this, coordinate transformation needs to be inherent in the deformation adjustment. Velsink [34] proposes to put every measurement

in the reference system of the first epoch. This transformation between reference systems is done in steps of 1 epoch, so for epoch n to epoch 1, $n-1$ transformations are needed. This means a set transformation parameters are needed for every epoch after the initial epoch 1. It also means there are no transformation parameters linking every epoch to every other. This prevents the amount of transformation parameters to increase exponentially with every epoch. And this method preserves the ability for a point in epoch 2 and a point in epoch 5 to be compared as they will both be in the coordinate system of epoch 1. In Equation 2.13 the symbolic equation of a single transformation is shown and in Equation 2.14 the symbolic equation of a transformations from epoch n to 1.

$$x_{n-1} = T_{n,n-1}(x_n, f_{n,n-1}) \tag{2.13}$$

$$x_1 = T_{2,1}(\cdots(T_{n-2,n-1}(T_{n,n-1}(x_n, f_{n,n-1}), f_{n-1,n-2}), \cdots f_{2,1}) \tag{2.14}$$

Where:

x_n = Parameters of measured point in epoch n
$f_{n,m}$ = Parameters of transformation from epoch n to m
$T_{n,m}$ = Transformation function from epoch n to m

Velsink [34] proposes that a general affine transformation equation can be used, as seen in Equation 2.15. The amount of parameters needed for a single general affine transformation is twelve. Affine transformation is a transformation in five aspects, namely translation, rotation, scaling, shearing and reflection. These aspects are visualized in 2D in Figure 2.6. The translation is captured in the translation vector and the other three aspects are captured in the matrix R.

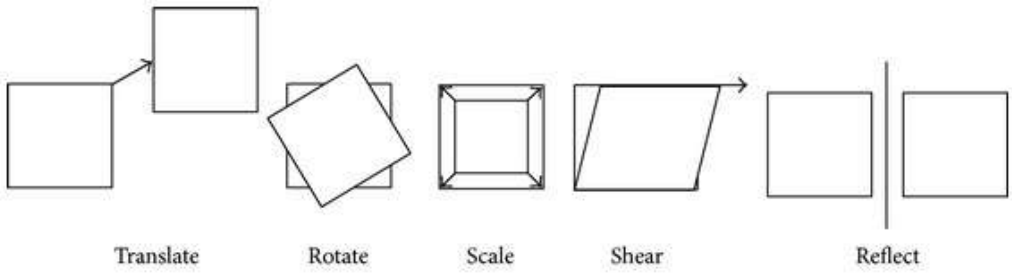

Figure 2.6: The five aspects of a affine transformation in 2D. Translation is a change in absolute position. Rotation is a change in orientation about the origin. Scale is a uniform change in size. Shear is a change in position proportional to the initial position. Reflection is a mirroring operation.[22]

Velsink [34] also states that other types of transformation can be achieved by putting constraints on this general affine transformation. For example, similarity transformation by constraining shearing or congruence transformation by constraining the shearing and scaling. These constraints will effectively decrease the amount of unknowns of the transformation from 12 to 6 unknowns for similarity and 7 unknowns for congruence, because constraints will act as observations and increase the degrees of freedom.

$$\begin{bmatrix}0\\0\\0\end{bmatrix} = -\begin{bmatrix}X_{to}\\Y_{to}\\Z_{to}\end{bmatrix} + R * \begin{bmatrix}X_{from}\\Y_{from}\\Z_{from}\end{bmatrix} + \begin{bmatrix}T_X\\T_Y\\T_Z\end{bmatrix} \tag{2.15}$$

where:

$$R = \begin{bmatrix}a_{11} & a_{12} & a_{13}\\a_{21} & a_{22} & a_{23}\\a_{31} & a_{32} & a_{33}\end{bmatrix} \tag{2.16}$$

Deformation in adjustment

The deformation equations in the deformation analysis will be between the transformed coordinate parameters in the adjustment. The deformation can be described by any equation with any amount of parameters. For example, the deformation equation can be a simple constant or a function of time and/or position.

2.3.2. Null hypothesis

After adjustment, the deformation hypothesis used in the adjustment can be tested. In deformation analysis, the null hypothesis is often the absence of deformation. This simplifies Equation 2.12 to Equation 2.17. The null hypothesis must be tested. For testing, Velsink [34] uses the Overall Model Test (OMT).

$$\underline{y} = A' x_s + \underline{e} \tag{2.17}$$

Overall Model test (Fisher-Test)

In the Overall Model Test (OMT), the null hypothesis H_0 is tested against the alternative hypothesis H_a, where H_a does not give any restrictions to the observations. This makes the OMT a general test of the null hypothesis, where only the residuals and covariance matrix need to be used [31].

$$F_{q=m-n,\infty} = \frac{\underline{T}_q}{\sigma^2} = \frac{1}{\sigma^2} \underline{\hat{e}}^T Q_y^{-1} \underline{\hat{e}} \tag{2.18}$$

Where:

$F_{q=m-n,\infty}$ = F distribution with dimensions q and ∞
$\underline{T}_q$ = OMT value of dimension q
$\underline{\hat{e}}$ = least-squares residuals
Q_y = observation covariance matrix
σ = square root of covariance factor

The OMT can reject the null hypothesis based on a critical value. The critical value is a boundary determined by the significance level, which is the probability for acceptance of a hypothesis. Setting a bad significance level can lead to a higher probability of wrongful rejection of hypothesis (Type-I error) or wrongful acceptance of a hypothesis (Type-II error) [14]. The significance level can be determined by the non-centrality parameter. This is known as the B-method [3, chapter 3]. In this way, tests of different dimension can have the same power γ and same non-centrality parameter λ_0 by changing the level of significance α. The non-centrality parameter is symbolically defined as:

$$\lambda_0 = \lambda(\gamma, \alpha, q) \tag{2.19}$$

where:

γ = power of the test (or probability of rejecting a false null hypothesis)
α = significance level
q = dimension of the test

It should be noted that the Overal Model Test does not give insights to the reason for rejection. Teunissen et al. [31] indicates that rejection could be from errors in observations, bad covariance matrix or an inappropriate null hypothesis. To get more insight other tests are needed.

W-test

The w-test is performed on a single observation of an adjustment. In the w-test the residual of the observation is evaluated against the stochastic distribution expected of that observation. The likeliness of that observation being correct is then returned from the w-test as a value. Like the Overall Model test (OMT), the test value of the w-test needs a critical value to be compared to. This critical value is determined by a set significance level. This significance level is the probability boundary, where an

observation is accepted. Meaning if a significance level of, say, 0.01% is used then if the observation is more likely than 0.01% the observation is accepted. The w-test is good for detecting blunders in the observations, however when dealing with many observations a problem occurs. At a 0.01% significance level with an adjustment of a million observations, a thousand observations should be rejected, which are not blunders just unlikely observations. In many adjustment application, as tacheometry and spirit-levelling, these amounts of observations are never reached, however in the photogrammetric adjustments millions of observations are easily reached.

2.3.3. Alternative hypotheses

If the null hypothesis is rejected, alternative hypotheses have to be made to find the deformation. Making alternative hypotheses is difficult as it requires assumptions of the deformation. Alternative hypotheses can be made using knowledge of the situation, physical mechanics causing the deformation or data-snooping.
One or more alternative hypotheses are tested using the Overall Model Test. With the multiple different alternative hypotheses, multiple tests have to be done. Every hypothesis can lead to a different amount of parameters in the adjustment. This changes the degrees of freedom. With a different degree of freedom, the critical value k_α of the test also changes, as the critical value is calculated using the dimension, power and non-centrality parameter of the test. Test statistics with different critical values can not be directly compared. To still be able to compare the Overall Model Tests the B-method of testing is used. In the B-method of testing, the test ratio, defined in Equation 2.20 [8] is used. This test ratio is comparable between test of different dimensions. In the B-method a standard power must be set and a reference non-centrality parameter must be calculated to make the critical value calculation solely a function of the dimension of the test.

$$T_R = \frac{T_q}{k_\alpha} \tag{2.20}$$

where:

T_R = test ratio
T_q = test statistic of dimension q
k_α = critical value

If this test ratio is bigger than 1 the hypothesis is rejected, as the test statistic is bigger than the critical value. For the test ratios that are below 1 the hypotheses can be accepted and the hypothesis with the smallest test ratio is assumed to be the best.

2.3.4. Application

The deformation analysis of Velsink [34] is gives a tested deformation estimation. Using photogrammetry in combination with this deformation analysis should be possible as the deformation analysis is build on a nonspecific general observation, which can be retrieved in photogrammetry. However, this analysis has not yet been applied using photogrammetry and difficulties will be possible. Can the adjustment be run in a reasonable time frame as there are much more observation using photogrammetry than for example levelling and tacheometry? Also, in the many observations there may be blunders. Is it possible to do the analysis when there are blunders in the observation, or can the blunders be worked around? Is the precision of the image point observations good enough to make the statistical tests significant at the millimetre level? Will the system reliably converge in the non-linear adjustment? Some adaptation may be needed to make the deformation analysis work reliably using photogrammetry these will be discussed in chapter 3.

3

Methodology

In this chapter, the methods are described to do photogrammetric measurements of a quay wall and process these measurements from multiple epochs to perform a deformation analysis. Starting from the acquisition of the measurements of the quay wall. Here, the aspects of the camera and measurement setup are discussed and the measuring process itself both for camera calibration and quay wall deformation. Then, the post-processing is discussed starting briefly with the feature detection processing. Followed by the single epoch adjustment where all approximate values are found for final non-linear multi-epoch deformation adjustment, which will be discussed last.

3.1. Acquisition

The photogrammetric measurements themselves may be simple pictures, but to use photogrammetry as an accurate measurment tool there are many aspects to take into account. These aspects, both general photogrammetry measurement aspects and quay wall specific aspects, are discussed in the following sections.

3.1.1. Camera specifications

The measurements can be made with normal digital camera with an objective lens costing a few hundred euros. This is a lens with a fixed focal length. Also, for photogrammetric application it is desirable to have a stable focal length and a stable lens distortion. As said in subsection 2.2.3 the intrinsics of an image contain the principal point, focal distance and lens distortion. These are calculated in the camera calibration procedure, which is explained in subsection 3.1.4. The calibration values are only valid for the lens used in the calibration. If the lens is not stable and changes, the calibration values are not valid any more. This means having a stable fixed focal length and a stable distortion is favourable as the estimated calibration is better applicable. Also, it is desirable to not have too much distortion to correct for with the intrinsics. This rules out using lenses such as a fish-eye for more field of view.

It is important to have a sharp image. Blurring in the images causes problems when trying to find features and match them between picture. Pinpointing the feature positions in blurry images is also less accurate and more inconsistent. This is especially important when using photogrammetry as an accurate measurement tool, where the aim is to get millimetre precision. Settings on the camera can help to get a sharp image. However, it is most convenient to keep the settings equal throughout the whole photo acquisition to make sure the calibration is also valid for all the measurements. First, a short shutter speed is good preventing motion blur. When the sensor is only exposed a short time the effect of camera shake and movement are minimized. Also, the aperture should be set to have good focus on all the objects in the image. The narrower the aperture of the camera is, the more the depth of field in the image. A bigger depth of field means objects at longer distance are sharp. However, a short exposure time and narrow aperture makes the image darker, so taking picture on bright conditions is advised. However, bright conditions can result in sharp dark shadows, which should be avoided. With the ISO (light sensitivity) setting the image can be made brighter, but a too high ISO introduces noise in the image. Shooting picture in RAW format is good as lighting can be adjusted after taking the picture.

3.1.2. Measurement Geometry

The size of a pixel in the terrain is an important specification to know. The feature detection precision is dependent on the size of pixels, which has a projected size in the scene. The projected size of a pixel in the scene is dependent on the distance between camera and photographed object, the focal length, and the size of a pixel on the sensor. This means that with closer objects, the projected pixel size is smaller. In aerial photogrammetry, the Ground Sampling Distance (GSD) is used to quantify this projected pixel size. The GSD is the length of a pixel projected on the ground. This can be adopted for Quay wall photogrammetry where instead of the ground the quay wall is used, creating the Wall Sampling Distance (WSD). This WSD can only be calculated for the images taken perpendicular to the quay wall as the WSD would not be constant in other image orientations. This is not a problem as the WSD is only used to get an indication of the size of an pixel in the 3D world. A small WSD is optimal to be able to have much detail and be able to precisely find features on the quay wall. To reach a small WSD the distance to the quay wall must be small, however this could give complications with overlap between images. The resolution and field of view have to be considered to make sure overlap is still enough for the photogrammetric process. With a higher resolution the distance to the wall can be increased as there are more pixels in a image. The distance increase leads to more overlap and need for less pictures. The field of view of a camera also makes that there is more overlap, but also makes it that the WSD increases as every pixel needs to cover more area.

This overlap can be calculated from the geometry of the pictures. A visual representation of the geometry is shown in Figure 3.1. First, the single image view of the quay wall can be calculated, using (mathematical) similarity between the triangle in the camera (using camera center and the sensor) and in front of the camera (using the camera center and the quay wall).

$$d_{view} = d_{sensor} * \frac{d_{wall}}{f} \tag{3.1}$$

where:

d_{view} = single image view range on wall
d_{sensor} = sensor width
d_{wall} = distance between camera and wall
f = focal length

Using the single image view, range and inter image distance, which represents the spacing between images, the overlapping area can be calculated.

$$d_{overlap} = d_{view} - d_{inter} \tag{3.2}$$

where:

$d_{overlap}$ = overlap between images
d_{view} = single image view range on wall
d_{inter} = image seperation

Combining Equation 3.1 and Equation 3.2, gives the equation for overlapping distance from the camera specific focal length and sensor width and distance to the quay wall.

$$d_{overlap} = d_{sensor} * \frac{d_{wall}}{f} - d_{inter} \tag{3.3}$$

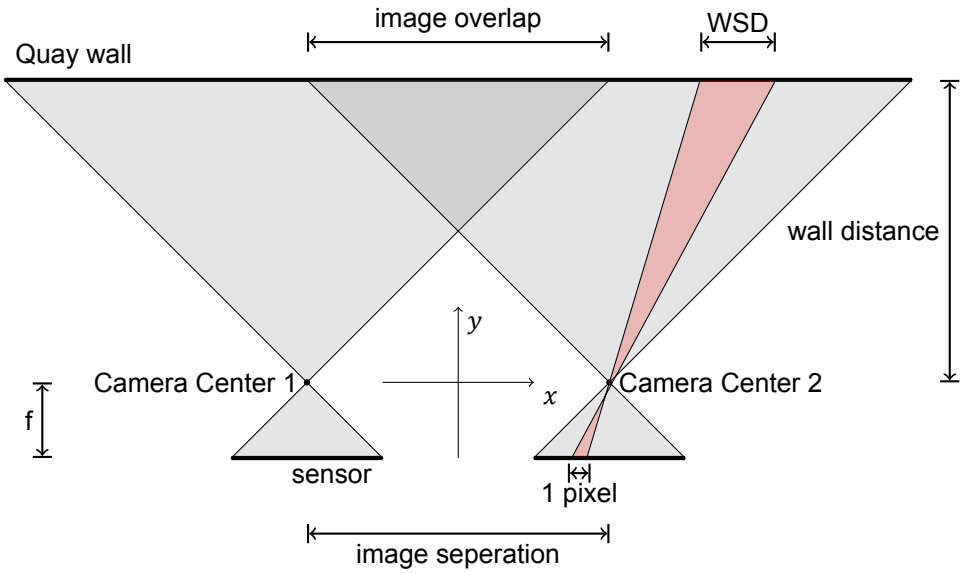

Figure 3.1: Schematic overview of the measurement geometry of a two images taken perpendicular to a quay wall. This figure both shows the image overlap geometry between images and the Wall Sampling Distance (WSD) geometry, which is the projected size of a single pixel on the quay wall.

The formula for the wall sampling distance (WSD) is similar to Equation 3.1, but instead of the entire sensor, a single pixel is taken to get the projected view of the pixel instead of the whole image.

$$WSD = d_{pixel} * \frac{d_{wall}}{f} \tag{3.4}$$

where:

WSD = Wall Sampling Distance, projected size of a pixel on the quay wall
d_{pixel} = pixel width
d_{wall} = distance between camera and wall
f = focal length

3.1.3. Measuring a quay wall

Tacheometric measurements are needed to retrieve coordinates of the reference points for the photogrammetry. This can be in any coordinate system, as there will be a coordinate transformation in the deformation analysis. This integrated transformation places every epochs measurements in the coordinate system of the first epoch. For use in photogrammetry, these tacheometric measurements must be made of points also captured by the photogrammetry, however the photogrammetric points are retrieved from image feature detection in processing and so are unknown during the measurements. To solve this, reference plates are made with markers, which are easily recognisable by computer vision. In this way there are marker points in the images that are known to be detected. Such a reference plate is shown in Figure 3.2.

Figure 3.2: A reference plate for the photogrammetric measurements. The reference plate has four round barcode markers, which have a numbering and can be pinpointed using computer vision. Also there are three orange prisms present, which are very accurately and reliably measurable by tacheometer.

Computer vision can not only pinpoint the marker position in an image, the identification number of the marker can also be read. The four markers of every reference plate are used by the photogrammetric processing to place all images and points in 3D space using a region growing-like process, which is described in section 3.3.

There are four markers on the reference plate and three prisms. Tacheometers are able to measure the markers directly, however the prisms make the tacheometric measurements more accurate and consistent and they are measurable at sharper angles. The prisms are better for the laser distance sensor, due to the great reflectivity of the prisms and the prisms reflect well even at sharper angles. Additionally with tilting prisms the angles can be even sharper when the prism is tilted towards the tacheometer. Being able to do sharper measuring angles allows for less positions from which the tacheometry has to measure. Having less tacheometer positions results in a great decrease in needed time to measure, as every tacheometer position needs not only to measure points for photogrammetry but also needs reference measurements to place the tacheometer itself and this takes time. Using prisms for the tacheometry means the markers need to be linked to the prisms. This is done using separate mea-

surements of the relative offset between prisms and markers from a tacheometer at close range. With these offset measurements the translation between prisms and markers is made.

The reference plates are placed on the quay wall with 50 meters between subsequent plates. After all reference plates are placed the images can be taken. The images are made from a boat moving parallel along the quay wall at a five meter distance from the wall, as seen in Figure 3.4. The whole quay wall can be captured in one run along the wall. About 100 pictures are taken every 50 meters, which gives much overlap. There are however multiple runs done along the quay wall, where in the different runs different orientations of the camera are used. As having multiple orientations improves the measurement geometry and the overlap between the images. While the imaging of the quay wall is being carried out, a surveyor measures in the markers/reference plate prisms using the tacheometer from the other side of the canal.

(a) Straight

(b) Upside-down

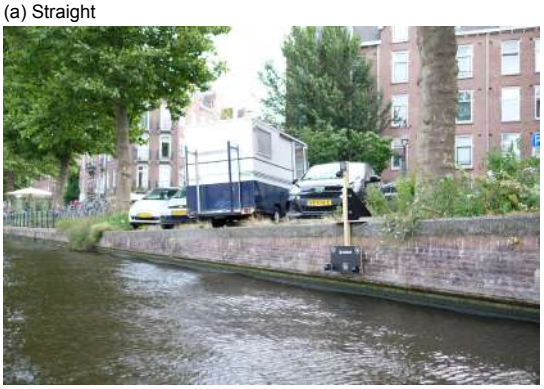

(c) Angled left

(d) Angled right

(e) High and angled down

(f) Farther away

Figure 3.3: Images with the different image orientations used to improve measurement geometry

Figure 3.4: Picture of the process of imaging the the quay wall. The boat is sailing parallel to the quay wall at approximately 5 meter distance.

3.1.4. Camera Calibration

The camera intrinsics are retrieved by a camera calibration procedure. In this procedure, an adjustment is done using a set of images picturing accurately identifiable markers, where the aim is too calculate the camera interior parameters. These interior parameters include the focal distance, pricipal point and the lens distortion model. In this procedure it is important to have observations well distributed over the image as the calculated interior parameters need to be accurate over the whole image. For lens distortion the Brown's radial distortion model with decentering [5] is used as described in subsection 2.2.3. The lens distortion formulas in Equation 2.8 and Equation 2.9 cannot be used directly for two reasons. Firstly, The Brown model assumes that the principal point is in the image center, at image coordinate $(0, 0)$. In practice the principal point has an offset from the image center. The Brown model can be adapted with three substitutions to work with a principal point offset.

$$dx = x - x_p \tag{3.5}$$

$$dy = y - y_p \tag{3.6}$$

$$dr = \sqrt{dx^2 + dy^2} \tag{3.7}$$

The second change to the Brown model is to make lens distortion balanced by setting a radius around the principal point where the radial distortion polynomial crosses zero [18]. This radius r_0 is called zero crossing and it is often taken to be in the range of $\frac{2}{3}$ to the maximum image radius [21]. The balanced lens model equation is made by subtracting the value of the polynomial at r_0 from the polynomial. The polynomial evaluated can be seen as an extra A_0 element of the radial distortion (Equation 2.3).

$$A_0 = A_1 r_0^3 + A_2 r_0^5 + A_3 r_0^7 + \dots \tag{3.8}$$

$$\begin{aligned} \Delta r &= -A_0 + A_1 r^3 + A_2 r^5 + A_3 r^7 + \dots \\ \Delta r &= A_1 r^3 - A_1 r^3 + A_2 r^5 A_2 r_0^5 + A_3 r^7 - A_3 r_0^7 + \dots \\ \Delta r &= A_1 (r^3 - r_0^3) + A_2 (r^5 - r_0^5) + A_3 (r^7 - r_0^7) + \dots \end{aligned} \tag{3.9}$$

These two additions to the Brown model are applied to Equation 2.8 and Equation 2.9 and the radial lens distortion parameters after A_3 are not taken into account as these will be negligibly small. The final lens model, can be seen in Equation 3.10 and Equation 3.11.

$$\Delta x = \delta x_r + \delta x_t = P_1(dr^2 + 2dx^2) + 2P_2 dxdy + dx * (A_1(dr^2 - r_0^2) + A_2(dr^4 - r_0^4) + A_3(dr^6 - r_0^6)) \tag{3.10}$$

$$\Delta y = \delta y_r + \delta y_t = P_2(dr^2 + 2dy^2) + 2P_1 dxdy + dy * (A_1(dr^2 - r_0^2) + A_2(dr^4 - r_0^4) + A_3(dr^6 - r_0^6)) \tag{3.11}$$

3.2. Feature Detection

For feature point detection a SIFT algorithm is applied to the image set. After features in the images have been found and described. Feature points will be matched between overlapping images. Finding the overlapping images before matching the points results in less errors where features between non-overlapping images will be matched.

SIFT finds many feature points in the images, however the spreading of feature points over an image is not controlled by SIFT. SIFT gives the feature points of which it has the most confidence. This can result in areas in the image with very many points, while other areas in the image have no points. When points are very close to each other they are not uncorrelated, however in the adjustment they are assumed to be uncorrelated. This results in a misrepresentation in weights, which can result in incorrect statistics of the adjustment.

To combat the clusters of feature points in images, a new point thinning procedure is developed. In the thinning process, two aspects need to be taken into account. Firstly, points that SIFT recognises and matches in many images are very good for the adjustment model, so it is not desirable to remove these. Secondly, there should be points well distributed over the entire image for every image. If every image only uses a certain part of the image the adjustment would become very vulnerable to lens errors/inconsistencies in those parts. These aspect are taken into account by the following thinning procedure.

Firstly, the feature points are ordered from best to worst using the amount of images a feature occurs in as metric. A good point is well recognisable by the feature detector and thus present and matched in multiple pictures. The more picture occurrences a feature has, the better a features is. Then a iterative process over the points starts, from the best point to the worst. For every point it is evaluated if adding the point to the images adds extra information. A point adds information if it is located in a part of the image where no features are added yet. The image parts of made by splitting the image multiple times in width and height.

3.3. Single epoch adjustment

As the collinearity equations are non-linear, the least-squares problem uses linearised version of these equations in a non-linear least-squares adjustment. This means an initial approximate value for every parameter is needed as the non-linear least-squares is an iteratively improving estimation. In aerial photogrammetry, the initial parameter values can be retrieved from approximate measurements from GNSS and INS on the plane and from ground control points. For quay wall photogrammetry there are no approximate values available to use as initial values. There is no GNSS or INS linked to the camera. The initial approximate exterior parameters of the images have to be calculated using the images themselves.

The approximate values are calculated by a region growing-like algorithm using forwards and backwards intersection, which is developed for this research. Where, as described in subsection 2.2.4, forwards intersection gets 3D terrain point coordinates from multiple images and, as described in subsection 2.2.5, backwards intersection gets exterior parameters of an image using multiple points in the image. In the next section, the algorithm for getting approximate values for a single epoch adjustment is discussed first. In subsection 2.2.5, the backwards intersection calculation is described in more de-

tail. Forwards intersection is not discussed in detail as the forward intersection algorithm used was available from the resources of Geodelta.

3.3.1. Single Epoch Adjustment with perfect data

The algorithm starts with at least four points, which have known coordinates and are identified in at least two separate images. These are the first images to be placed using backwards intersection. Commonly, the backward intersection is also an iterative calculation. However, this would require initial values, which are not present. So, a closed-form backwards intersection method is used. This closed-form backwards intersection can calculate the exterior parameters of an image using four known points. A more detailed view of the closed-form backwards intersection calculation is discussed in Appendix A.

There have to be at least two images that are positioned in the first backwards intersections using the initial four points. The points (found by SIFT) which are in at least 2 placed images are selected. Forward intersection can be used on these images and their common points to place those points in 3D and so extend the amount of known points. With the expansion of the known points it may be possible to place more images with backward intersection. And with more images more points can be placed with forward intersection. This cycle continues alternating forward intersection to expand the known points and backwards to expand the known images. When all images and points are found. The point positions and image positions/orientations can be used as initial values for the non-linear Least Squares adjustment. Below (algorithm 1), a pseudocode overview of this process is shown.

Algorithm 1: Single Epoch Adjustment with perfect data

Input: Known 3D reference points & imagepoint observations for every image
Output: Image exterior parameters & 3D point coordinates

```
1  Find all images which have at least 4 known points;
2  Position those images by backward intersection;
3  if Amount of images placed < 2 then
4  |  Error: Can not continue;
5  else
6  |  Find all points which are present in at least 2 images;
7  |  Position those points by forward intersection;
8  while There are images which have at least 4 known points do
9  |  Position the image with most known points by backward intersection;
10 |  Find all points which are present in at least 2 images;
11 |  Position those points by forward intersection;
12 Non-linear Least Squares adjustment using Bundle;
```

3.3.2. Single Epoch Adjustment with imperfect data

There is one problem in algorithm 1. It assumes that the data is perfect. SIFT must perfectly find and pinpoint features and the features must be perfectly matched between images. In reality this is not the case. SIFT gives incorrect matches between images and also they are not perfectly pinpointed in the images. The images themselves also have geometric errors, for example, from light refraction. These errors make for a need to add robustness measures to the algorithm. This is done at multiple places in the algorithm.

The first robustness measure proposed to the newly developed single epoch adjustment is a point filter using the residuals from the forward intersection. The forward intersection algorithm uses a small least-squares adjustment in which residuals can be calculated. If these residuals are above a certain threshold the point is likely incorrectly placed, and thus the point is not kept. This does give an extra condition that the point has to be present in at least three known images, instead of two. This condition is already satisfied during the SIFT feature detection, as requiring a certain amount of feature occurrences is a good filter for SIFT features.

The second robustness measure proposed is a RANSAC approach to improve backward intersection. The backward intersection uses 4 points, however there may be many more known points in the image. Most likely some of the known points are incorrect. By doing the backwards intersection

many times using different sets of 4 known points many possible image exterior parameter sets can be determined. Then the best image position/orientation is chosen. The choice is based on the smallest projection error of the fourth point.

The third robustness measure is an intermediate non-linear least-squares adjustment. In every iteration after the forward intersection a non-linear least-squares adjustment is done using already found images and points. If this adjustment is successful, an Overall Model Test (OMT) is done. If this OMT is smaller than its critical value the newly placed image and points are approved. If the OMT is above the critical value, a w-test is used to filter out the bad observations corresponding to the incorrect points. If the OMT gets below the critical value after the w-test filtering, the newly placed image and points are approved. If the adjustment is not successful, then the newly placed image and points are rejected. Rejected images are first temporarily skipped. If later in the process they still can not be, placed they are permanently skipped and will not be placed. Below a pseudocode overview of the algorithm can be seen.

Algorithm 2: Single Epoch Adjustment with imperfect data

Input: Known reference points & imagepoint observations for every image
Output: Image exterior parameters & 3D point coordinates

```
Find all images which have at least 4 known points;
Position those images 1000-times by backward intersection using random
 4 known points;
Choose image position with smallest projection error; // Backward
 intersection robustness measure
if Amount of images placed < 2 then
    Error: Can not continue;
else
    Find all points which are present in at least 2 images;
    Position those points by forward intersection;
    for point in placed points do
        if residual < threshold then // Forward intersection robustness measure
            Accept point;
        else
            Reject point;
        end
    end
    Perform Non-linear Least Squares adjustment using all known images
     and points; // Intermediate adjustment robustness measure
    if Adjustment successful then
        if OMT < critical value then
            accept images and points placed;
        else
            while OMT > critical value do
                Filter points using w-test;
            end
        end
    else
        Error: Can not continue;
    end
    while There are images which have at least 4 known points do
        Position the image with most known points 1000-times by backward
         intersection using random 4 known points;
        Choose image position with smallest projection error; // Backward
         intersection robustness measure
        Select the image position with the smallest projection error;
        Find all points which are present in at least 2 images;
        Position those points by forward intersection;
        for point in placed points do // Forward intersection robustness measure
            if residual < threshold then
                Accept point;
            else
                Reject point;
            end
        end
        Non-linear Least Squares adjustment; // Intermediate adjustment
         robustness measure
        if Adjustment successful then
            if OMT < critical value then
                accept images and points placed;
            else
                while OMT < critical value do
                    Filter points using w-test;
                end
            end
        else
            Image and points rejected;
        end
    end
end
Perform Non-linear Least Squares adjustment using all known images and
 points;
```

3.4. Deformation

The Photogrammetric Deformation analysis workflow is based on the general deformation analysis from Velsink [34]. In section 2.3 this method is discussed in general in this section it will be discussed in connection to quay wall photogrammetry.

3.4.1. Single epoch adjustment to multi epoch deformation adjustment

The single epoch adjustment is done to extract the approximate values to make the non-linear deformation adjustment possible. For the deformation adjustment it is important to have points, which are identified in multiple epochs. The single epoch adjustment does not take into account this condition. This is solved with a new run of SIFT feature matching using the images of all epochs, which are placed in the single epoch adjustment. In this multi epoch SIFT matching points are found in the images with the condition that they are identified in multiple epochs. All image positions and orientations are now known from the single epoch adjustment and this can be used in the SIFT matching procedure to more quickly estimate which images overlap and thus where feature points can be matched. The newly found multi-epoch points for deformation also need approximate values in every epoch they are in, because all the image positions and orientations are already known there is no need for a region growing process like single epoch adjustment, because every new point can be immediately placed using forward intersection. In short, to prepare for multi epoch deformation adjustment extra SIFT points are found and placed, which are identified in multiple epochs and thus can be used to calculate the deformation.

3.4.2. Deformation Adjustment

Observation vector y

The y observation vector is formed. In this vector all observation values are stored. A observation is a value with a certain uncertainty, which is the stochastic nature of the observation. This uncertainty is defined in the $D(y)$ covariance matrix, using the variances of the observations on the diagonal and covariances between the observations on the non-diagonal positions.

$$y = \left[a_1, b_2, \dots, b_p, f, d\right]^T \tag{3.12}$$

where:

- a_1 = image point observation values vector for epoch 1
- b_2 = image point observation values vector for epoch 2 approximately transformed to a's reference system
- b_p = image point observation values vector for epoch p approximately transformed to a's reference system
- f = transformation constraint observation vector = $\vec{0}$
- d = deformation constraint observation vector = $\vec{0}$

The observation vector is split in three groups. First the image observations (a_1, b_2 and b_p), which link the image extrinsics, image intrisics to the terrain point by the collinearity equations as seen in Equation 2.1 and Equation 2.2.

The second group are the transformation constraints, which are the zero observations. They link points $P_{A,n}$ in epoch n to their transformed point $P_{A,n-1}$ in epoch $n-1$ using a transformation equation with parameters $f_{n,n-1}$.

$$0 = T(P_{A,n}, P_{A,n-1} f_{n,n-1}) \tag{3.13}$$

The third group are the deformation constraints, which are zero observations. They link points $P_{A,1}$ to points $P_{B,1}$ by a deformation equation with parameters ∇. $P_{A,1}$ and $P_{B,1}$ are they same point measured at different epochs, but transformed to the coordinate system of the first epoch.

$$0 = D(P_{A,n}, P_{B,n}, \nabla) \tag{3.14}$$

Parameter vector x

The parameter vector x is formed from the parameters in all the observation equations. These are all the 3D terrain point coordinates and their transformed versions, all the exposure station extrinsics and intrinsics, the transformation parameters and the deformation parameters. They are all put in the x parameter vector.

$$x = \left[c, f, \nabla\right]^T \tag{3.15}$$

where:

c = linearised observation equation (collinearity) parameter vector
f = transformation parameter vector
∇ = deformation parameter vector

Design matrix A

Due to the non-linear nature of the observation/constraint equations, linearisation is needed to make the design matrix A. Linearisation of the observation equation means that the observations and parameters in the least-squares adjustment will be adjustments to the observations and parameters of the previous iteration. This means instead of y and x, the least-squares adjustment uses observation adjustments Δy and parameter adjustments Δx.

$$\Delta y = \left[\Delta a_1, \Delta b_2, \dots, \Delta b_p, \Delta z_f, \Delta z_d\right]^T \tag{3.16}$$

where:

Δa_1 = adjustment of observation values vector epoch 1
Δb_2 = adjustment of observation values vector epoch 2
Δb_p = adjustment of observation values vector epoch p
Δz_f = adjustment of transformation constraint observations = 0
Δz_d = adjustment of deformation constraint observations = 0

$$\Delta x = \left[\Delta c, \Delta f, \Delta \nabla\right] \tag{3.17}$$

where:

Δc = adjustment of linearised observation equation (collinearity) parameters
Δf = adjustment of transformation parameters
$\Delta \nabla$ = adjustment of deformation parameters

The A matrix is built from the linearised observation equations linking observations and parameters. A schematic overview of the A matrix of a two epoch deformation adjustment can be seen in Figure 3.5.

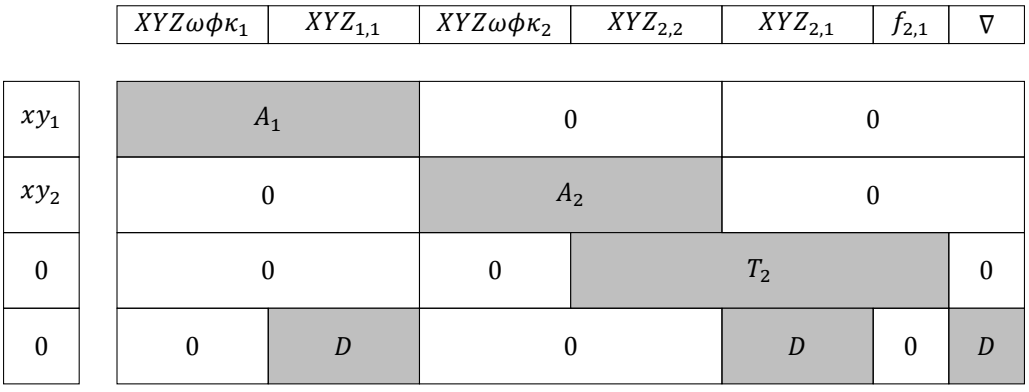

Figure 3.5: Schemetic overview of the structure of a deformation adjustment design matrix using measurements from 2 epochs. Parts A_n contain the linearisation of the image point observation equation (collinearity equations), which links the observations xy_n to the image parameters $XYZ\omega\varphi\kappa_n$ and point parameters $XYZ_{n,n}$, where n is the epoch. parts T_n contain the linearisation the transformation equation, which links the point parameters $XYZ_{n,n}$ to the point parameters $XYZ_{n,n-1}$ using the transformation parameters $f_{n,n-1}$, where n is the epoch. Parts D contain the linearisation of the deformation equations, which links point parameters $XYZ_{n,1}$ to point parameters $XYZ_{m,1}$ using the deformation parameters ∇, where n and m are different epochs.

All the way on the left are the observations xy_n for both epochs and the 0 observations for the transformation and deformation constraints. On the top there are the parameters with the image extrinsics and intrinsics $XYZ\omega\varphi\kappa_n$, the terrainpoints $XYZ_{n,n}$ the translated terrainpoint $XYZ_{n,n-1}$, the transformation parameters $f_{n,n-1}$ and the deformation parameters ∇. In the A_n parts of the A matrix the single epoch adjustments are done. In the T_n part of the matrix the points from epoch 2 are transformed to the coordinate system epoch 1. In the D parts of the matrix the deformation between points in epoch 1 and transformed point from epoch 2 is added.

3.4.3. Adjustment

First, the Δy vector is determined by subtracting the calculated observation values from the y observation vector. The calculated observation values use the last iteration's parameters or the initial approximate parameters in the first iteration. Using the linearised observation equations the A design matrix is formed.

The $\Delta\hat{x}$ parameter adjustment is then calculated using the least-squares formula:

$$\Delta\hat{x} = (A^T Q_y^{-1} A)^{-1} A^T Q_y^{-1} \Delta y \tag{3.18}$$

The parameter adjustment $\Delta\hat{x}$ is then added to the last iteration's parameters x to make new adjusted parameters $\hat{x}$. The improvement from the iteration is calculated. If that improvement is smaller than a certain threshold the adjustment is complete and the iterating stops.

3.5. Deformation Adjustment program

Geodelta has a program called *Bundle*, which can perform adjustments for a photogrammetric system of equations. *Bundle* is limited to single-epoch adjustments and so for estimating the deformation this program has to be extended. This extension includes integrating an epoch number to every observation/parameter and many additional observation and parameter types. The initial state of *Bundle* included the following observation types:

- Imagepoint, an imagepoint actually consist of two observation an imagepoint x-observation and y-observation. These observation are the image coordinates of the projection of a terrain point on the image. The observation equation is deducted from the collinearity equations. The parameters in this observation equation are:
  1. Image extrinsics, which consists of six parameters. Three parameters for the position of the image X_c, Y_c, Z_c and three parameters for the orientation of the image ω_c, ϕ_c, κ_c
  2. Image intrinsics, which consists of at least 3 parameters. These three parameters are the focal distance of the camera used and it's principle point x and y coordinates. Additionally when a lens distortion model is used more parameters have to be added. For example in the Brown radial lens distortion model two or three parameters are added.
  3. Terrain point position, the 3D position of the terrain point.
- Distance constraint, a distance constraint consists of an observation of a distance between two terrain points. The observation equation of the constraint is the euclidean distance between the two terrain points. The only six parameters in this equation are then the 3D positions of both terrain points.
- Observed coordinate, an observed coordinate consist of three observations. The three observation are the X, Y and Z coordinates of a terrain point. The observation equations are simple the observed terrain point coordinate value is equal to the parameter coordinate value of that terrain point. This means every observation equation has one parameter, the parameter is the observation.

Bundle is also able to do the different adjustment phases to fullfill the procedure described by Polman and Salzmann [24]. In this procedure first a phase one adjustment, also known as free network adjustment, is done and then a phase two adjustment, also known as adjustment to control points. In the free network adjustment only observations are used. The position, orientation and scale of the system

is determined by the S-basis (Schrankingsbasis in Dutch). The S-basis consists of a minimal amount of constraints to set this position, orientation and scale. The minimal amount of constraints is 7 as the scale (1 parameter), 3D positions (3 parameters) and 3D orientation (3 parameters) need to be set. The free-network adjustment is used to statistically test the observations, for example by means of overall model test (F-test) or w-test. With this adjustment bad observations can be filtered out. In the second phase adjustment with control points is done. Additionally to the observations, known control points are added to the adjustment system. These control points are given a a priori standard deviation just like the observations. With enough control points to reach 7 parameters the system is fixed in space and the S-basis is not needed. This means that the coordinate system of the adjustment result is determined by the control point coordinate system. To make the *Bundle* program able to handle a multi-epoch deformation measurements additions to the program are made. The observation types added are:

- Transformation constraints, a transformation constraint also consists of three non-stochastic zero observations. One observation for every axis in the 3D space. The observation equation is the Affine transformation (rewritten to be equal to zero). The Affine transformation has six parameters. Three parameters are the translation and three parameters are the rotation.
- Deformation constraints, a deformation constraint consists of a non-stochastic zero observations. The observation equation is the relation between a terrainpoint in two different different epochs. There are at least six parameters in this equation. These six parameters consist of three parameters for both terrain points. More parameters are possible as it depends on the deformation model (function) used. For example, if the deformation model a an nth degree polynomial, there will be n more parameters. Or if the deformation model is a constant value, 1 parameter will be added.

3.5.1. Affine Transformation Observations & Parameters

In Equation 2.3.1, the transformation as intended by Velsink [34] for deformation adjustment is described. In this research a transformation embedded in the adjustment as Velsink [34] proposes. However, instead of using the general affine transformation with constraints to make a congruence transformation, a different transformation is used to remove the need for the constraints as they are built into the matrix. This is done by using a rotation matrix $R(\omega, \varphi, \kappa)$. This rotation matrix uses the three euler angles to determine the entire nine element matrix. The rotation matrix can be seen in Equation 3.19 and the total transformation formula with this rotation matrix in Equation 3.20.

The total transformation uses 6 parameters to transform a point to another coordinate system. Linking a pair 3D points between coordinate systems gives 3 observations (X,Y,Z). Meaning with at least two pairs of points linked coordinate transformation can be calculated assuming that the points are known.

$$R(\omega,\varphi,\kappa) = \begin{bmatrix} cos\kappa * cos\varphi & cos\kappa * sin\varphi * sin\omega - sin\kappa * cos\omega & cos\kappa * sin\varphi * cos\omega + sin\kappa * sin\omega \\ sin\kappa * cos\varphi & sin\kappa * sin\varphi sin\omega + cos\kappa * cos\omega & in\kappa * sin\varphi * cos\omega - cos\kappa * sin\omega \\ -sin\varphi & cos\varphi * sin\omega & cos\varphi * cos\omega \end{bmatrix} \tag{3.19}$$

$$\begin{bmatrix} 0 \\ 0 \\ 0 \end{bmatrix} = -\begin{bmatrix} X_{to} \\ Y_{to} \\ Z_{to} \end{bmatrix} + R(\omega,\varphi,\kappa) * \begin{bmatrix} X_{from} \\ Y_{from} \\ Z_{from} \end{bmatrix} + \begin{bmatrix} T_X \\ T_Y \\ T_Z \end{bmatrix} \tag{3.20}$$

3.5.2. Deformation Observations & Parameters

The deformation equation are equations, where two points of different epochs, but in the same coordinate system are linked. Which deformation equations are used is the deformation hypothesis. The null hypothesis in a deformation adjustment should be the absence of deformation. This leads to the most simple deformation equation, which is ”no deformation”. This means a point is stable and thus its coordinates are the same. This will result in the following vector equation.

$$\begin{bmatrix} X_{A1} \\ Y_{A1} \\ Z_{A1} \end{bmatrix} = \begin{bmatrix} X_{A2} \\ Y_{A2} \\ Z_{A2} \end{bmatrix} \tag{3.21}$$

However, in the deformation adjustment the deformation observation are non-stochastic zero observations so the equation is rewritten to have a zero vector on 1 side. This is also done for all following deformation equations.

$$\begin{bmatrix}0\\0\\0\end{bmatrix} = -\begin{bmatrix}X_{A1}\\Y_{A1}\\Z_{A1}\end{bmatrix} + \begin{bmatrix}X_{A2}\\Y_{A2}\\Z_{A2}\end{bmatrix} \tag{3.22}$$

If there is deformation and the null hypothesis of ”no deformation” is rejected, then alternative deformation hypothesis are needed. These alternative deformation hypothesis use any deformation equation. A basic example of such an deformation equation is a unique constant value deformation between epochs. Where for every coordinate a unique value is added to represent the deformation. The vector equation can be seen below.

$$\begin{bmatrix}0\\0\\0\end{bmatrix} = -\begin{bmatrix}X_{A1}\\Y_{A1}\\Z_{A1}\end{bmatrix} + \begin{bmatrix}X_{A2}\\Y_{A2}\\Z_{A2}\end{bmatrix} + \begin{bmatrix}dX_{1-2}\\dY_{1-2}\\dZ_{1-2}\end{bmatrix} \tag{3.23}$$

4

Results

In this chapter the results of two tests will be discussed. The first is a wooden mock quay wall test. This test evaluates the deformation estimation accuracy and precision as the deformation applied to the mock quay wall is approximately known and some deformation points are measured by a tacheometer. This means there are deformations to compare to the photogrammetric deformation estimation. The second test is the measurement of the Schinkelkade in Amsterdam. In this test a real quay wall is measured 4 times with a month interval between the measurements. It is not known if this wall will deform between measurements. However it is expected that this quay wall will not move. This test evaluates the deformation analysis process with real quay wall data and find if application is possible in practice.

4.1. Wooden mock quay wall test

Figure 4.1: Mock quay wall test setup. The two wooden boards represent a quay wall. The boards are moved and tilted by which a deformation is simulated.

In this test, the quay wall consists of two wooden walls with barcodes on them. The walls are moved to simulate a deformed quay wall. The test setup using the mock quay wall is shown in figure Figure 4.1. With this test setup multiple deformations are tested. An overview of the different tests is shown in

Table 4.1. The deformations are always applied to the right wall, the left wall is not deformed in any test as control. This means the left wall should always show a 0 mm deformation in all results. There are a few control points needed in every epoch to fix that epoch in 3D space. The same six barcodes are used for every epoch. These barcodes are located on the outer frame on the mock quay wall. In every test, the X-direction is horizontally parallel to the wall, the Y-direction is horizontally perpendicular to the wall and the Z-direction is vertical.

Test	Deformation type	Deformation X	Deformation Y	Deformation Z
1	Tilt	No deformation	Tilted 3 mm	No deformation
2	Tilt	No deformation	Tilted 5 mm	No deformation
3	Tilt	No deformation	Tilted 58 mm	No deformation
4	Tilt	No deformation	Tilted 84 mm	No deformation
5	Tilt	Tilted 14 mm	Tilted 84 mm	Tilted 15 mm
6	Translation	Translated -32 mm	Translated 24 mm	Translated 15 mm
7	Translation	Translated -32 mm	Tilted 24 mm	No deformation
8	Tilt/Translation	Unknown	Unknown	Unknown

Table 4.1: Overview of the simulated deformation tests using a wooden mock quay wall. The deformation of the wall in every test is stated for the three principal directions, namely horizontal along the wall (X), horizontal perpendicular to the wall (Y) and vertical (Z). This stated deformation is the deformation in the right wall, as the left wall is never deformed as control.

As an extra comparison, the barcodes in the corner of the right wall are also measured using a tacheometer. For every epoch an adjustment is done using the tacheometric measurements. The difference of the adjusted 3D coordinates of the corner barcodes between epochs is retrieved to get the tacheometric deformation estimation. The photogrammetry also uses the barcodes as deformation points. This means there is a deformation estimation of the same point using the photogrammetry and tacheometry, which is used to compare the deformation estimations.

4.1.1. Estimated Deformation

To estimate the deformation, the hypothesis is used that all the barcodes on both the left and right wall are deforming with a unique value in X, Y and Z direction. The smaller barcodes on the frame are assumed stable in the hypothesis. The coordinate system used in all epochs is the same. This means that the rotational and translational transformation parameters are 0. The coordinate transformation between epochs will be estimated in the deformation adjustment, so these are expected to be 0.

During adjustment a problem occurs where the iterations were only slightly converging and the adjustment never reached the threshold to stop iterating. When the rotation parameters of the transformation are fixed to be zero the adjustment does converge. The deformation results with fixed rotations are the similar as with estimated rotations. The deformation of the points only differs in the order of 0.001 mm. This means this convergence problem only has effect on the transformation estimation. For the further deformation evaluation of the tests, it is chosen to fix the rotations. Otherwise, the non-stochastic transformation observations heavily influence the Overall Model test.

Tilting tests

The first five tests were focussed on tilting the right wall. An overview of the expected and estimated deformations of these tilting test is given in Table 4.2. Figure 4.2 only contains Y-deformations of the right wall as the left wall was not deforming on purpose. In this left wall only submillimeter deformation were found in every test. As the expectation is no deformation in the left wall a submillimeter deformation is a good result.

The estimated deformations of the right wall are similar to the expected applied deformations, as deformation in the order of millimeters were found with good accuracy. When tilting the wall the deformation should linearly change. The tilting Y-deformation should linearly increase from bottom to the top of the wall, as the top off the wall is moved forwards or backwards. In tests 1, 2, 3, 4 and 5, there is a tilted deformation in the Y direction, where this linear trend is visible as seen in Figure 4.2. Even the small deformations from test 1 and 2 are accurate. An additional tilt in the X direction is tested in tests 4 and 5. Here, the X-deformations are accurate to what is expected. In tests 1, 2 and 3, there is also a

small deformation in X (submillimeter for test 1 and 2 and max 3 millimeter for test 3) even though no deformation is expected. However, these are small deformations and they are due to the imprecision of moving the wall, which becomes worse the more the wall is moved. This means the tests where the wall is moved multiple centimetres in Y direction (3,4,5) the other directions will also de deformed by some millimeters. Lastly, an additional tilt in the Z direction is tested in test 5. Here, the Z-deformation is also accurate to what is expected. In the other tests where no Z-deformation is expected only small deformations are found. This small deformation is caused by the tilting of the plane, because tilting a plane in the Y-direction, also results in the points on the plane slightly moving down. Overall, the five tilting tests show that the estimated deformations are within a few millimeters to the expected deformations, where the small differences are attributed to uncertainty in measurement and expectation.

Test	Row	Expected X Deformation in mm	Estimated X Deformation in mm	Expected Y Deformation in mm	Estimated Y Deformation in mm	Expected Z Deformation in mm	Estimated Z Deformation in mm
1	Bottom	0	0.01	0	0.21	0	-0.04
1	Top	0	-0.33	3	3.27	0	0.13
2	Bottom	0	0.01	0	-0.06	0	0.04
2	Top	0	0.39	5	5.22	0	0.17
3	Bottom	0	0.10	0	3.41	0	1.04
3	Top	0	2.95	58	58.83	0	3.72
4	Bottom	-1	-0.79	33	29.50	0	1.32
4	Top	2	2.05	84	85.07	0	3.84
5	Bottom	4	1.55	33	24.83	0	2.85
5	Top	14	14.70	84	83.94	15	14.30

Table 4.2: Overview of estimated vs. expected deformation in the tilted plane deformation tests. The range of deformations expected and estimated is shown for every test in X, Y and Z direction.

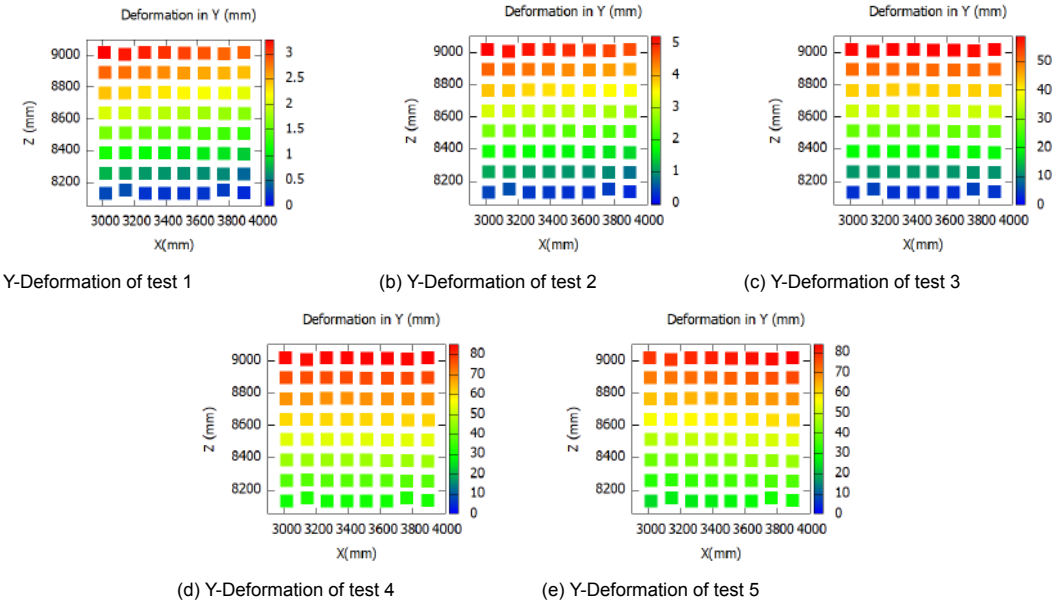

(a) Y-Deformation of test 1

(b) Y-Deformation of test 2

(c) Y-Deformation of test 3

(d) Y-Deformation of test 4

(e) Y-Deformation of test 5

Figure 4.2: 2D front view of the wooden mock quay wall, where the deformation points on the wall are coloured to the size of their deformation in a Y direction. These tests were done with tilted plane deformation. The description of the deformations for every test are found in Table 4.1. The deformations in X and Z direction are visualized for these tests in Figure B.1

Translation tests

Tests 6 and 7 were focussed on a translation of the wall. Instead of the linearly changing deformations in the tilting tests, these translation tests should give a deformation that is equal for every point on the wall. An overview of the results of the translational tests is given in Table 4.3 and in Figure 4.3 the deformations of the tests are shown. Figure 4.3 only shows the right wall as the left wall was not

deforming on purpose.

For test 6 and 7 the right wall was mainly translated. A translational Z-deformation should be present in test 6. In test 6 the expected deformation in Z is found accurately. For test 7 there is a discrepancy between the expected and estimated deformation. The expected deformation is 0, however there is a linearly increasing deformation from 0 to -5 mm. This looks similar to the tilted deformations of test 5. This is a mistake in the logging of the test setup. The Z-deformation was achieved by removing 5 mm wooden planks from under the wall. In test 7, 3 wooden planks should have remained on both sides of the wall this would give no Z deformation as the wall in image set 1 also had 3 planks underneath. However, 4 planks were underneath one side of the wall making it 5 mm higher than the other side. This created the linearly changing Z-deformation as seen in the estimated Z-deformation. The estimated Y-deformation is accurate to the expected deformation in both test 6 and 7. Overall, the two translational tests show that the estimated deformations are similar to the expected deformations, where the small differences are be attributed to uncertainty in measurement and expectation.

Test	Row	Expected X Deformation in mm	Estimated X Deformation in mm	Expected Y Deformation in mm	Estimated Y Deformation in mm	Expected Z Deformation in mm	Estimated Z Deformation in mm
6	Bottom	-32	-33.38	24	22.49	15	11.48
6	Top	-32	-31.72	24	26.06	15	12.93
7	Bottom	-32	-34.63	-2	-2.24	0	-0.01
7	Top	-32	-34.25	22	20.87	0	5.80

Table 4.3: Overview of estimated deformation and expected deformation in the translated plane deformation tests. The range of deformations expected and estimated is shown for every test in X, Y and Z direction.

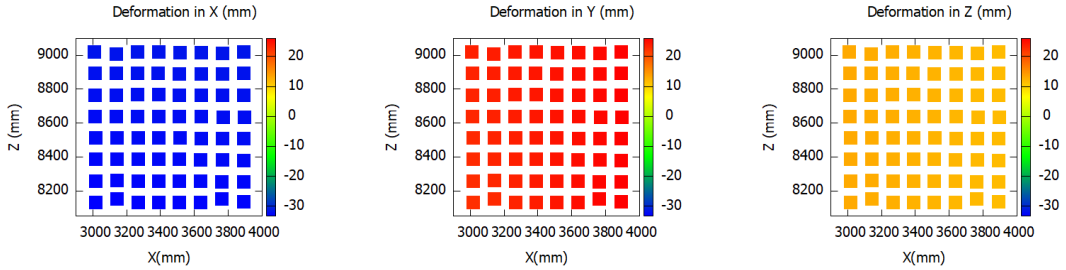

(a) Deformations of test 6

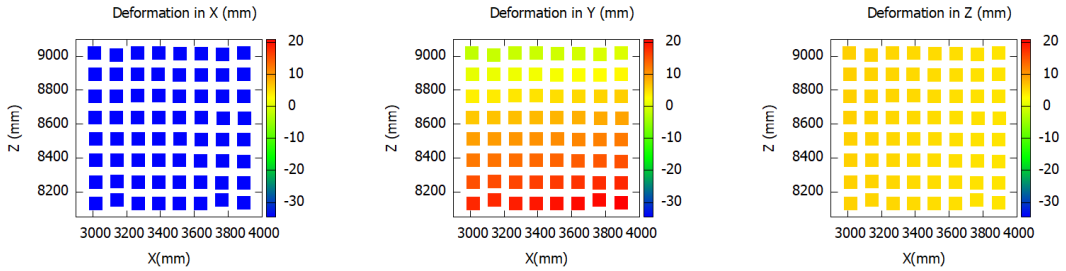

(b) Deformations of test 7

Figure 4.3: 2D front view of the wooden mock quay wall, where the deformation points on the wall are coloured to the size of their deformation in a X, Y or Z direction. These tests were done with translated plane deformation. The description of the deformations for every test are found in Table 4.1.

Tacheometry Comparison

Barcodes in the corners of the right wall are also measured by tacheometer and a deformation is retrieved from these measurements. For every epoch the tacheometric measurements were put in an adjustment and the differences between the adjusted 3D coordinates of the barcodes is taken as deformation. This is also how the quay wall deformation monitoring is done currently in Amsterdam. In

Figure 4.4 three plots are shown with the estimated deformations from tacheometry vs. photogrammetry. The exact numbers used in these plots can be found in Table B.1, where the estimated deformations using tacheometry and photogrammetry and the difference between those deformation are listed. In this comparison test 9 is also used. This test was not mentioned in the previous sections as the deformation in this test was not logged, so it was not possible to make an expectation. The deformation in test 9 was measured using tacheometry and photogrammetry, so it is included in this comparison.

Both the deformation estimations have an uncertainty. The Tacheometer has a precision of about 0.5 millimeter. The tacheometric measurements are done in close-range (< 10 meter), however the barcodes are not ideal for a tacheometer to measure. The photogrammetric measurements are assumed to have a precision of one pixel. Using Equation 3.4 with a distance of 5 meters to the wall and a pixelsize of 0.0039 millimeter, the size of this precision on the wall is estimated. This results in an expected photogrammetric precision of 0.8 millimeter on the wall.

The difference in deformation estimations between photogrammetry and tacheometry is small. For the X- and Z-deformations the difference is less than 0.5 millimeter. The difference between the Y-deformation is only slightly bigger with a maximum of 0.8 millimeter. These small differences are within the precision of the measurements, which are 0.5 millimeter and 0.8 millimeter for tacheometry and photogrammetry respectively. This means in this test the photogrammetric deformation are as good as the tacheometric measurements. As tacheometry is the currently used method of deformation monitoring this is a good indication that photogrammetric deformation monitoring is a capable alternative. The slighlty bigger difference in Y-deformation could be a result of the measurement geometry of photogrammetric measurements. Images are only taken from the front of the wall, which makes the precision in the Y-direction worse. This effect is also seen on the real quay wall, as discussed in subsection 4.2.2.

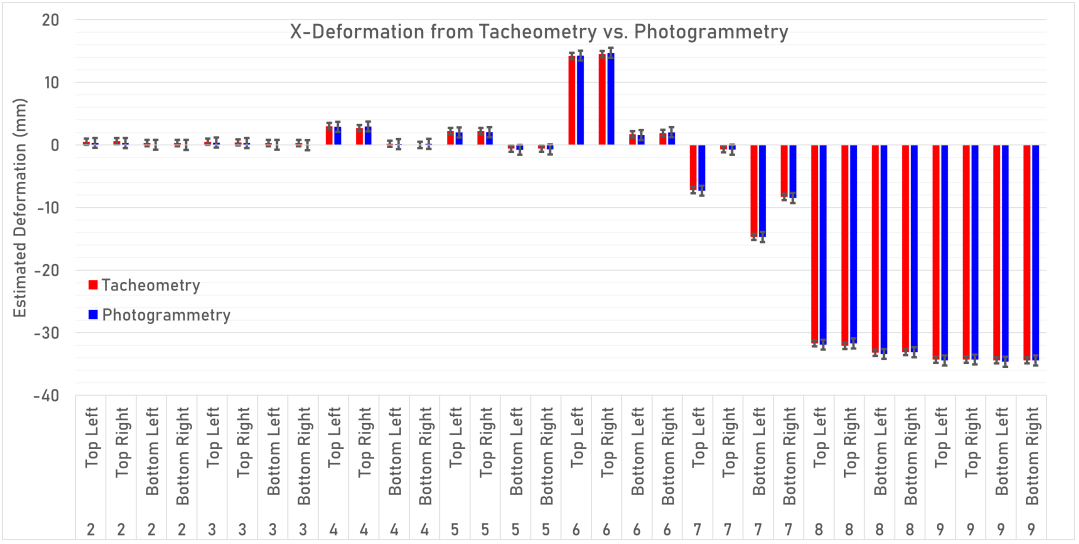

(a) The estimated X-deformations (Y-axis) in the barcodes at the corners of the mock wall for every test (indicated by test number and corner description on the X-axis) from tacheometry and photogrammetry with error bars, which indicate the expected precision of the estimations, which is 0.5 mm for tacheometry and 0.8 mm for photogrammetry.

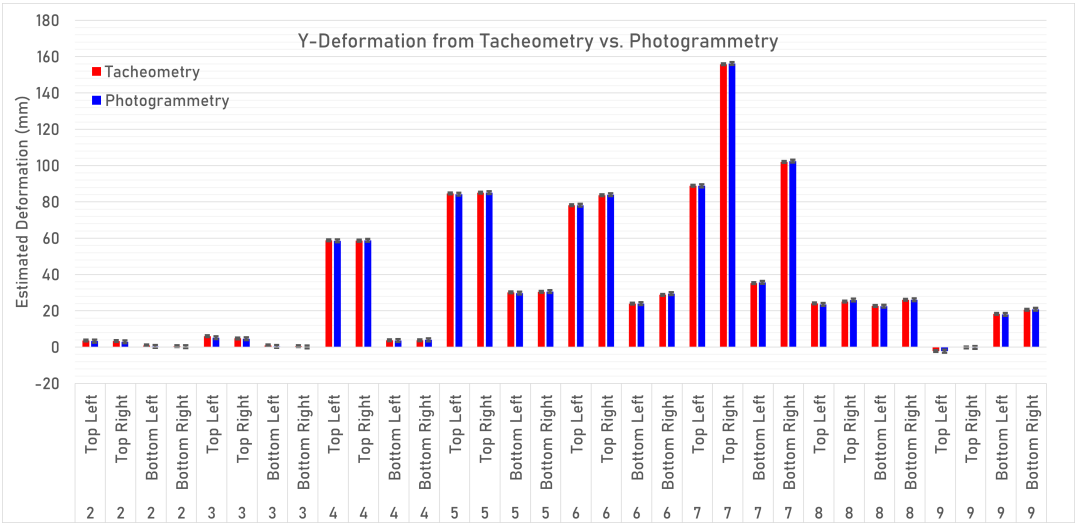

(b) The estimated Y-deformations (Y-axis) in the barcodes at the corners of the mock wall for every test (indicated by test number and corner description on the X-axis) from tacheometry and photogrammetry with error bars, which indicate the expected precision of the estimations, which is 0.5 mm for tacheometry and 0.8 mm for photogrammetry.

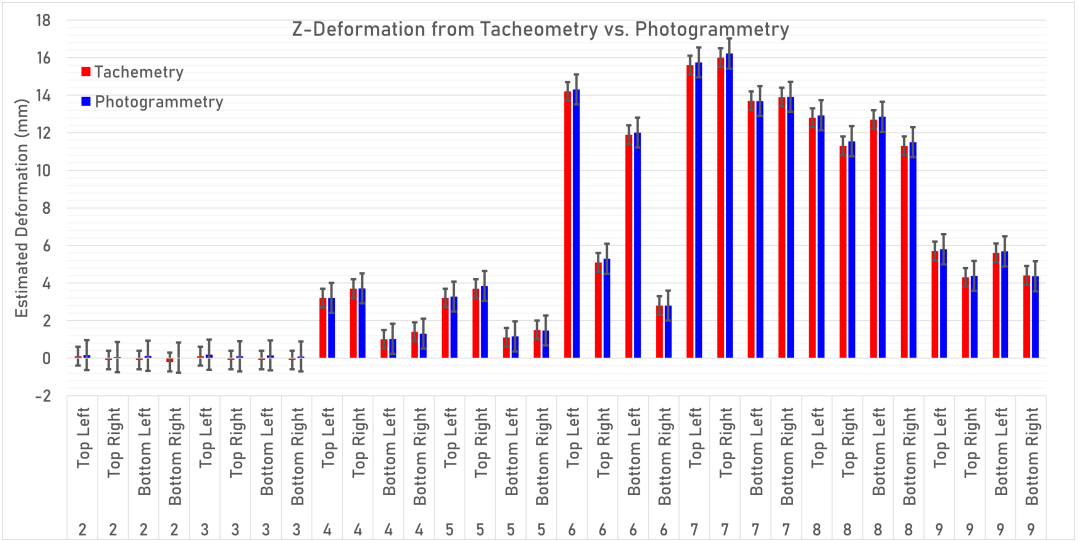

(c) The estimated Z-deformations (Y-axis) in the barcodes at the corners of the mock wall for every test (indicated by test number and corner description on the X-axis) from tacheometry and photogrammetry with error bars, which indicate the expected precision of the estimations, which is 0.5 mm for tacheometry and 0.8 mm for photogrammetry.

Figure 4.4: Plot for comparison between the tacheometric and photogrammetric estimated deformations in X, Y and Z directions. The tacheometry show a very similar estimated deformation in all measurement points where the difference between tacheometry and photogrammetry is within the precision of both techniques.

4.2. Amsterdam Schinkelkade test

Multi-epoch test measurements are made at the Schinkelkade in Amsterdam for the development of the photogrammetric deformation analysis of quay walls. This test is done by Geodelta in collaboration with Bouwrisk. In this test photogrammetry and tacheometry are used.

4.2.1. Measurements

In Table 4.4 an overview of the Schinkelkade measurements is shown along with the epoch number they are assigned. In the timespan of this research it was possible measure and process 4 epochs.

Epoch	Date	Nr. of images	Orientations
1	5-3-3021	1085	straight (5 meter), left, right, upside-down, high
2	19-4-2021	1184	straight (5 meter), left, right, upside-down, high
3	11-6-2021	1080	straight (5 meter), left, right, upside-down, high, straight (10 meter)
4	9-7-2021	811	straight (5 meter), left, right, upside-down, high, straight (10 meter)

Table 4.4: Overview of the Schinkelkade meausrements with date of measurement and assigned epoch number.

The workflow of this test is separated in two parts, the workflow of the tacheometric deformation monitoring and the workflow of the photogrammetric deformation monitoring. For the tacheometry, surveyors perform the usual monitoring procedure. One surveyor places prisms on set points on the quay wall at approximately 10 meters interval. These set points are on top of the wall and at the bottom and top of the front face of the wall. Some of these bottom points make it necessary to use a boat to place the prisms. The other surveyor operates the total station on the other side of the canal to measure in the prisms. Every prism needs to be measured from different positions and every position of the total station needs to be referenced from known reference points placed on the surrounding buildings.

The workflow of the photogrammetric monitoring starts with placing the reference plates. The spacing between the reference plates is set at approximately 50 meters. After the reference plates are placed additional markers are placed in some of the set points for the tacheometry prisms on the quay wall. These additional markers are not necessary for the photogrammetric deformation analysis, however it is useful to have common points between the tacheometry and photogrammetry and these additional markers are measurable by both methods. The additional markers are, like the markers on the reference plates, detectable and identifiable by computer vision.

The reference plate barcodes and additional markers are measured in by the tacheometer. As mentioned in subsection 3.1.3, prisms are used to reach a better accuracy. In the first epoch smaller static prisms were used on the reference plate instead of the tilting prisms seen in Figure 3.2, which were used from epoch 2 on. The prisms of epoch 1 were less accurate and not reliably measurable from sharp angles, which lead to the need for more tacheometer positions, which then leads to time needed to measure the quay wall.

In the measurements of epoch 1 and 2, multiple runs at five meter along the quay wall are done with different camera orientations, as explained in subsection 3.1.3. The orientation used were straight, angled left, angled right, upside-down and from above. For the third and fourth epoch an extra run was done at ten meters from the quay wall with a straight camera orientation. This ten meter run made the single epoch adjustment, where the approximate image and point positions are estimated, much easier. The extra images made for much extra overlap between images also between image not directly next to each other. This made it possible for the process to skip a hard-to-place image without the algorithm getting stuck.

4.2.2. Single epoch adjustment Schinkelkade

To eventually do the deformation adjustment, first the approximate values of all parameters (points positions and image orientations/positions) need to be estimated and a single epoch adjustment is performed. The single epoch adjustment is done following the method described in section 3.3. From the single epoch adjustment a point cloud is extracted containing the adjusted terrain points. Also, the a

posteriori standard deviation of these points are retrieved from the adjustment and added to the point cloud. The a posteriori standard deviation is seen as the precision in the coordinates.

This precision is estimated for X,Y and Z direction for every point in the adjustment, where X is the horizontal direction along the quay wall, Y is the horizontal direction into the quay wall and Z is the vertical direction. The point cloud with point precisions is visualized for the single-epoch adjustment of epoch 3 in Figure 4.5, 4.6 and 4.7. These figures show that the standard deivation of the points on the quay wall are mostly below 1 millimeter for X- and Z-direction and mostly below 1.5 millimeter of Y-direction. As images can only be taken from the front on the quay wall the depth in Y-direction is harder to estimate. This is similar to GNSS, which has a worse height estimation due to measurement geometry, because measurements can only be taken from above.

The millimeter precision of single epoch adjustment points is a good indication that the deformations estimated in the multi epoch adjustments will be good enough to assess deformations of 15 mm, as required. The precision of the points on the buildings behind the quay wall are much worse, mostly more than 2.5 mm standard deviation. This is the reason why there are no deformations estimated using these points in the next processing step.

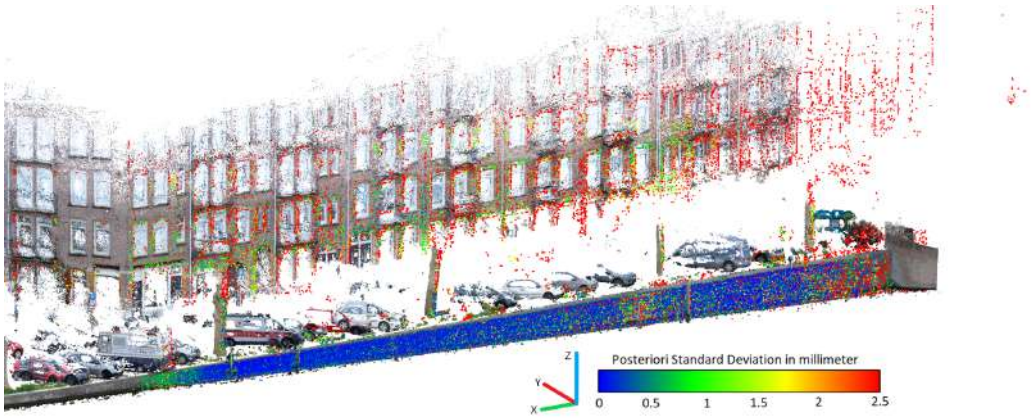

Figure 4.5: Point cloud with points of epoch 3. The points are coloured to the a posteriori standard deviation in X direction, which is the direction horizontal along the quay wall.

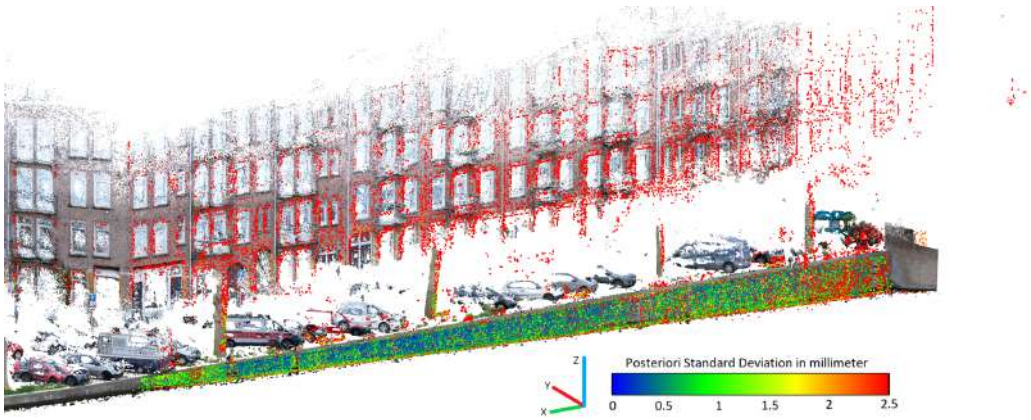

Figure 4.6: Point cloud with points of epoch 3. The points are coloured to the a posteriori standard deviation in Y direction, which is the direction perpendicular to the quay wall.

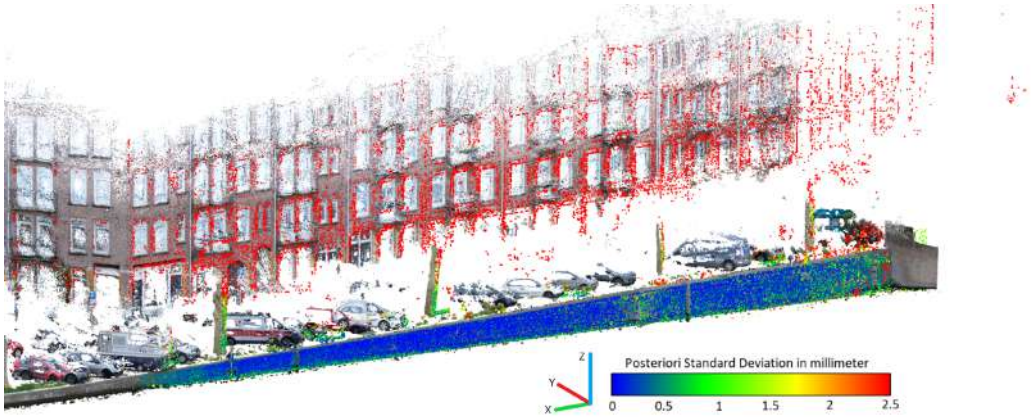

Figure 4.7: Point cloud with points of epoch 3. The points are coloured to the a posteriori standard deviation in Z direction, which is the direction vertical along the quay wall.

4.2.3. Deformation adjustment

First, a deformation analysis between epoch 1 and 3 is done from one reference plate to the next reference plate in parts. This means the quay wall is split in parts of approximately 50 meters. This is done to increase the speed of the total process. Also, it makes it easier to detect where potential errors occur. For a more in depth analysis of the adjustment the first part of the Schinkelkade quay wall is chosen, as this part has the highest quay wall and so more points on the wall, which make the statistics more reliable.

In Table 4.5, a summary of the size of the system is shown. There are 118 344 terrain points in epoch 1 and 3 combined. The points present in both epochs are the deformation points, i.e. the points where an deformation is estimated. When selecting the deformation points, an additional condition is set that a deformation point must be a point on the quay wall. This is done as the deformation in the points on the houses is not of importance and they are not accurate as the precision in these points is worse, as mentioned in subsection 4.2.2.

Number of	**”no deformation” hypothesis**	**”with deformation” hypothesis**
Images	374	374
Points	118 344	118 344
Control Points	16	16
Image points	794 299	794 299
Observations	1 680 191	1 680 191
Parameters	406 795	448 885
Degrees of Freedom	1 231 306	1 273 402

Table 4.5: Size of the adjustments with ”no deformation” hypothesis and ”with deformation” hypothesis.

Hypotheses and testing

The deformation adjustment in the analysis has two parts. First the adjustment uses the null hypothesis, only if the null hypothesis is rejected then alternative hypotheses will be used. For the deformation analysis the null hypothesis states, there is no deformation in the quay wall. This hypothesis is enforced in the adjustment through the non-stochastic deformation observations. The ”no deformation” equation of a point is seen in Equation 3.22. After the adjustment the Overall Model test (OMT) is calculated to test if the null hypothesis is valid. The ”no deformation” hypothesis gives a OMT of 0.173 with a critical value of 1.004. This OMT is accepted and thus ”no deformation” is valid. Technically this means that the conclusion of this deformation analysis is that the quay wall is not deforming. However, for evaluation purposes of the deformation analysis, an alternative hypothesis with deformation is also used.

The alternative ”with deformation” hypothesis assumes that the quay wall is deforming. The deformation model is the most simple possible, namely every deformation point individually deforms with no relation to the other points. The ”with deformation” equation of a point is seen in Equation 3.23. This adjustment is done and the OMT is calculated to be 0.156 with a critical value of 1.004. This OMT is also accepted and thus this ”with deformation” hypothesis is valid.

For evaluation purposes, the ”with deformation” alternative hypothesis is compared to the ”no deformation” null hypothesis. In practice only alternative hypothesis should be compared to each other , however the analysis currently only integrates one altnerative hypothesis and so no comparison would be possible. The (unrounded) critical values of the adjustment with and without deformation is different as the dimension of the test is different. The dimension of the OMT is equal to the degrees of freedom and, as seen in Table 4.5, the ”with deformation” hypothesis gives more parameters, namely 42 090 extra deformation parameters. These parameters are the X, Y and Z deformations for 14 030 deformation points on the part of the quay wall. The test ratio’s of the ”no deformation” and ”with deformation” adjustments are 0.172 and 0.155, respectively. This means that the ”with deformation” hypothesis is slightly better than the ”no deformation” hypothesis. This is however due to a bias in the test ratio comparison. Even though the differences in critical values due to different degrees of freedom are taken into account by the test ratio, there still is bias to hypotheses, which are more loose. This means there are parameters in the adjustment with less strict observations. The ”with deformation” hypothesis has loose deformation parameters as each deformation parameter is dependent on a single deformation observation.

Deformation estimation

From the ”with deformation” adjustment, the deformation estimates are retrieved. These deformations are plotted in 3D space at the position of the deformation point in the first epoch. For reference a dense point cloud is added. This is shown in Figure 4.8, 4.9 and 4.10. The deformation points are coloured according to the deformation in a certain direction.

From the deformation adjustment the following deformation are retrieved. An estimated X-direction deformations are between -2 mm and 1 mm. An estimated Y-direction deformations are between -1 mm and 1 mm. An estimated Z-direction deformations are between -3 mm and 0 mm. It should be noted that these deformation retrieved from points that are between reference plates and thus control points. Deformation points not between control points are not as accurate. These point are extrapolated while points between reference plates are interpolated, which is more reliable. Overall, the deformations estimated between the control points in all direction are small enough to assume the quay wall is stable.

Figure 4.8: Point cloud with deformation points. The deformation points are coloured to the deformation in X direction, which is the direction horizontal along the quay wall. The position of the reference plates with control are indicated with an arrow.

Figure 4.9: Point cloud with deformation points. The deformation points are coloured to the deformation in Y direction, which is the direction perpendicular to the quay wall. The position of the reference plates with control are indicated with an arrow.

Figure 4.10: Point cloud with deformation points. The deformation points are coloured to the deformation in Z direction, which is the direction vertical along the quay wall. The position of the reference plates with control are indicated with an arrow.

Observation residuals and W-test

From the adjustment, the final observation residuals are retrieved. The residuals of the image point observations are the difference between the adjusted observation and the original observation. Every image point observation has a x- and y-component. The image point residuals are plotted in two histograms, one for x-residual and one the y-residual. Over these histograms a fitted normal distribution of the residuals is plotted. The expectation of the residuals is a normal distribution as this is also chosen as stochastic distribution for the image point observations. The means of these fitted distributions are -2.92×10^{-8} mm and -1.51×10^{-8} mm for x and y residuals, respectively. This is close to zero, which means the observations are accurate. The standard deviation is 0.0017 mm for both x and y residuals. The expected standard deviation, which is also given as the a priori standard deviation of the observations, is 1 pixel, which is equal to 0.0039 mm on the camera used. This means that with 0.0017 mm the standard deviation of the fitted distribution over the residuals shows that a better precision is reached than expected.

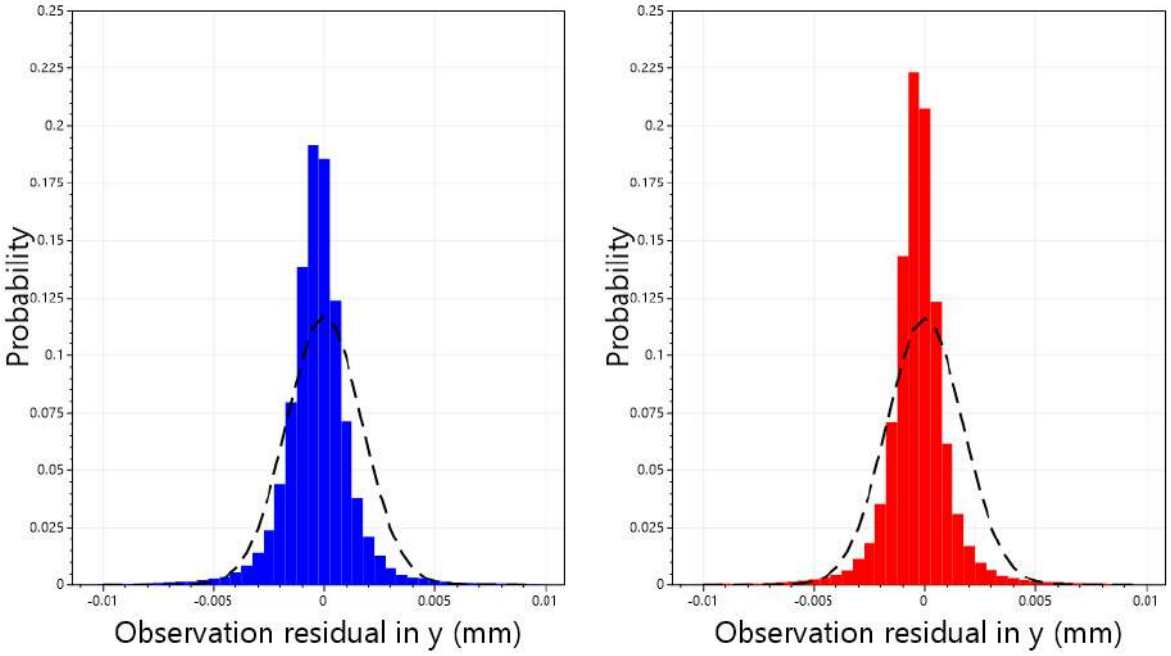

Figure 4.11: Histograms of image point observation residuals in x and y after adjustment

The adjustment residuals are also used to perform the individual observation w-tests. However, these calculations require the inverse of the matrix $A^T A$. As described in Equation 3.4.2, the matrix A has as many columns as parameter in the adjustment and as many rows as observations in the adjustment. With millions of observations and hundred thousands of parameters the $A^T A$-matrix is large and calculating the inverse is a computational intensive process. Processing a 50 meter part of the quay wall already requires 4 hours to take the inverse. This is the reason why these w-tests are calculated with thinned observations. The thinning is done using the algorithm explained in section 3.2.

It should be noted that these big inverses are not necessary for the deformation estimation and hypothesis evaluation by the Overall Model Test. Only the individual observation w-test calculations require this much time and so this computation size problem is not important.

The advantage of the w-test compared to looking at the residuals is that all the observations that are evaluated can be compared even when they have a different stochastic distribution. The w-test is set to reject an observation if the chance of that observation is less than 0.1 percent. In the deformation analysis millions of observations are made, which means there is an expectation to have rejected observation, as explained in Equation 2.3.2. This is shown in the histograms in Figure 4.12. By far the most w-test values are below the critical value of 3.29. This critical value is derived from the 0.1 percent chance of a observation being an outlier. The frequency of w-test values quickly decreases with a higher w-test value, which shows that the observation are good relative to their stochastic nature. With more than 100 000 observations in this histogram it is expected to have a hundred rejected observation and this is also the case. This does really not harm the deformation analysis as there will be thousands of deformation points on the quay wall and a few possible outliers will not change the ability to see a trend of a deforming wall.

Of course, there could be real blunders among the observations, which is why it is good to have a option to check these observations. Photogrammetry gives as a good way to check observations. Every image point observation comes from a point on an image. These are visually verifiable by plotting on the image, if it is needed. For example, if a suspected blunder appears to be in the water when looking at the observation in the image, it is verified that this observation in a blunder. An example of observations plotted in the image is shown in Figure 4.13.

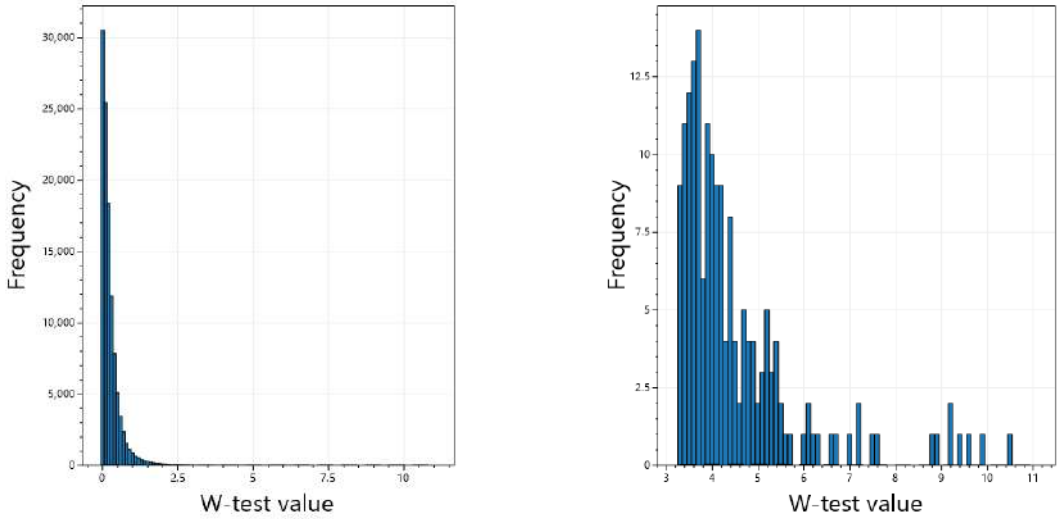

(a) Histogram of the w-test values of all observations

(b) Histogram of w-test values above critical value of 3.29

Figure 4.12: Histogram of observation w-test values. In figure a, it is shown that most w-test values are mainly at zero and the frequency of observations with an bigger w-test is quickly declining. In figure b only observations with a w-test value bigger than the critical value of 3.29 are shown. Here it is visible that there are not many observations with w-test value above the critical value compared to the thousands of observations in figure a with a w-test value below the critical value.

An advantage of the w-test for deformation adjustment is it does not only test the many image point observations, but also the transformation and deformation observations. If these observations are rejected, then there is a good reason to check if there are not any mistakes in the adjustment. These transformation and deformation observation rejections can come from incorrect deformation hypothesis or mismatched points.

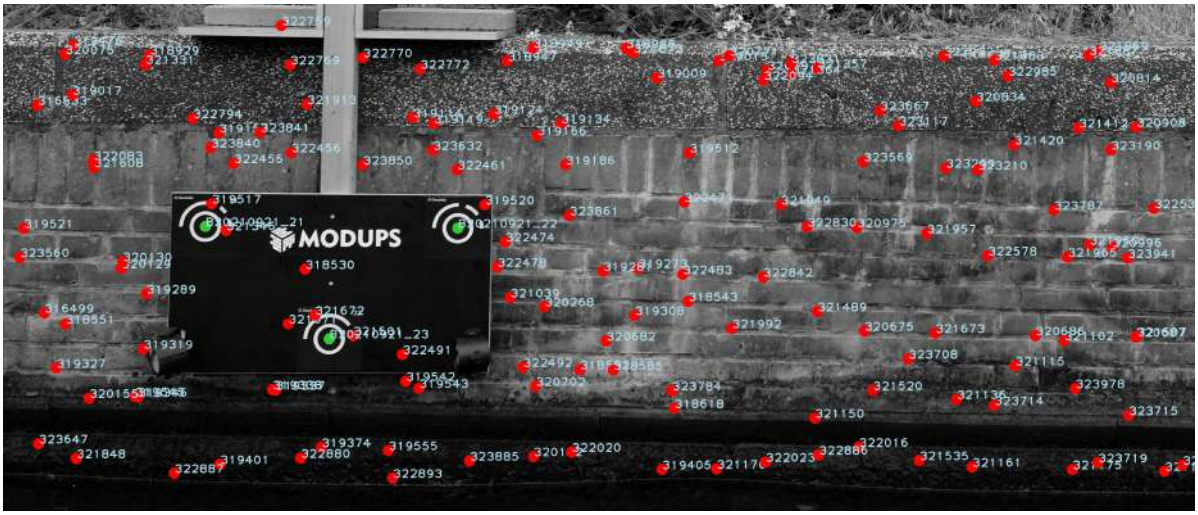

Figure 4.13: Part of an image used in the deformation analysis with some observations plotted in the image. Observation positions are presented as coloured dots with a name in the image. The name is used so an observation of the same point is identifiable in multiple images. Sift observations are the red dots and barcode observations are the green dots. The image has been turned to grayscale to make the coloured dots and labels more visible. The image has more more observations than shown, however plotting all observations will impede the clarity

4.2.4. 250 meter wall deformation

When more than 50 meters of quay wall are used in the deformation analysis, the individual observation testing will take too much time to compute, as the design matrix of the adjustment becomes too big to invert. This means individual observation testing will not be done for these quay wall deformation adjustments.

It is found that measurements of epoch 1 and 2 gives problems. Epoch 1 has difficulties in the last 50 meters of the quay wall and epoch 2 has difficulties in the first 50 meters of the quay wall. In both these difficult parts, the single epoch adjustment of their respective epochs is not connecting the control reference plates well enough to make a reliable adjustment. This seemed to be solved in epoch 3 and 4 where an extra set of images from 10 meter to the quay wall was used. This extra set of images obtained at a greater distance is improving the overlap between pictures and this makes the single epoch adjustment easier. The focus will be on the epochs 3 and 4 for the larger deformation analysis.

In Figure 4.14 and 4.15 the deformation estimations between epoch 3 and 4 are visualized. The Schinkelkade is not expected to move so the deformation should be around 0, however it is not certain that the quay wall will not move.

The estimated deformations in X direction show a deformation of -2 to 2 mm. This deformation is mainly caused by a waving trend in the deformation along the quay wall. This could be a systematic error or actual deformation. Most probable is a systematic error as it is seen that at every reference plate the deformation is approximately zero, while at the reference plates the errors in the estimation should be smallest. Also, the wave pattern seems consistent over the whole wall. This systematic error is suspected to come from an imperfect calibration. An imperfect calibration can be caused by an improper calibration measurement, in which case better care should be taken when calibrating, or an incorrect calibration model, which does not model the lens distortion well enough, in which case a different calibration model or different camera should be used.

The most important deformation direction for quay wall stability is the Y-direction into the quay wall. The estimated deformations in Y direction show a deformation of -1 to 3 mm. There is a part of the wall indicated by the gray box in Figure 4.14, where there may be a small deformation in the Y -direction. The estimated deformations in Z direction show a deformation of -1 to 1 mm. There are no notable features in this deformation direction, the wall is very stable in Z-direction

Overall the deformations show that the quay wall, which is not expected to be deforming, is barely moving with maximum deformations of -2 to 3 mm. With this range estimated deformation it will be possible to reliably detect deformation on a a quay wall, which is deforming 15 mm or more.

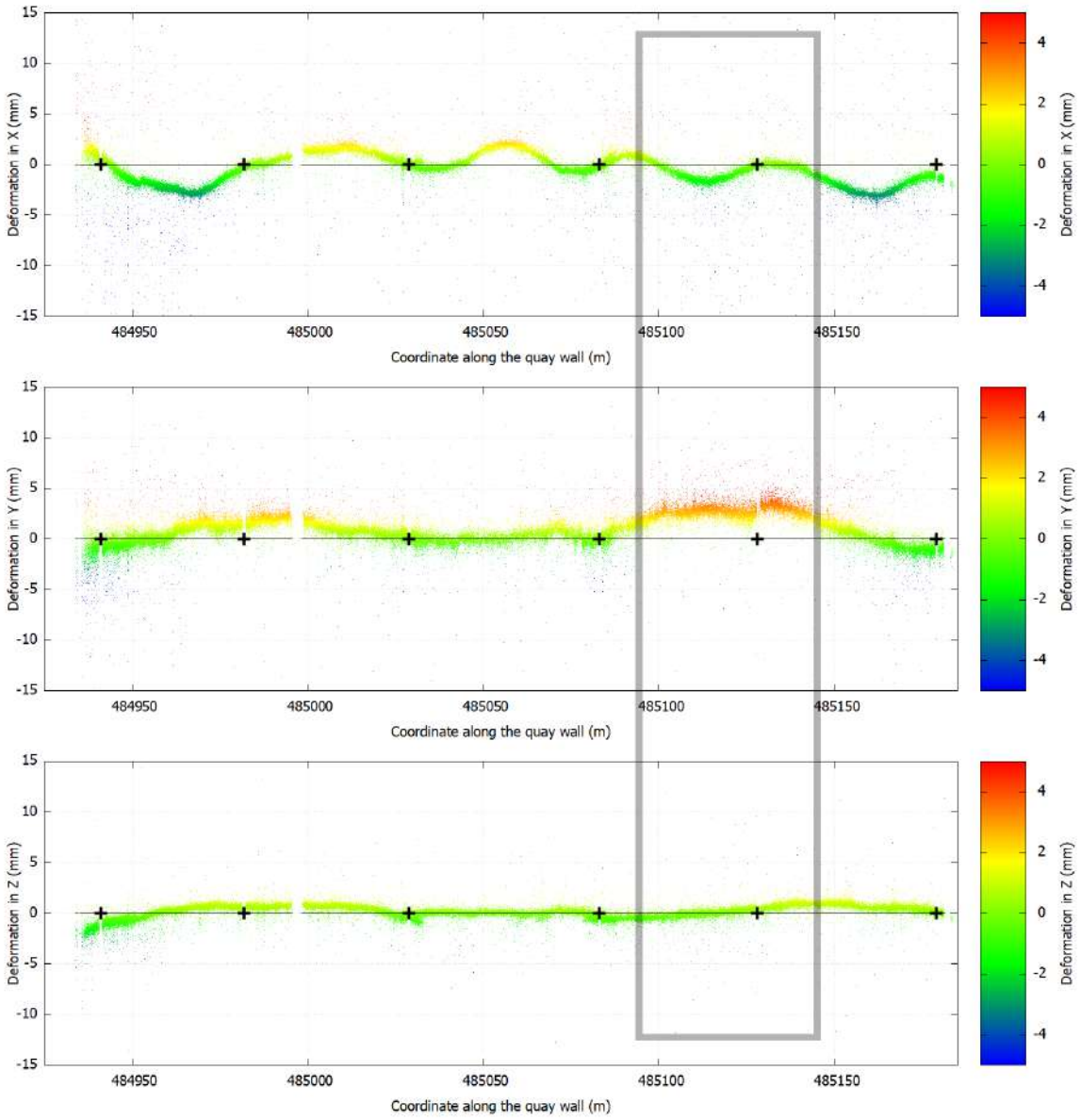

Figure 4.14: Plot of the deformations in X, Y and Z direction along the quay wall. The plot Y-axis is the size of the deformation in a certain direction and the X-axis are the position of the deformation points along the quay wall. Horizontal black line is the zero deformation line and the + markers indicate locations of the reference plates with the control points. A gap in the plot means no points are deformation points are present.

(a) Estimated X-deformation between epoch 3 and 4

(b) Estimated Y-deformation between epoch 3 and 4

(c) Estimated Z-deformation between epoch 3 and 4

Figure 4.15: Estimated deformation between epoch 3 and 4. Deformation points are coloured to the deformation size in X-, Y- or Z-direction with a dense point cloud for visualization purposes of 250 meters of quay wall at Schinkelkade in Amsterdam.

5

Discussion

In this chapter, the results presented in chapter 4 will be discussed and interpreted to reach answers to the research question asked in section 1.3. Starting by discussing the quality of the deformation estimation retrieved from photogrammetry. Followed by a discussion on the improvements in time cost and coverage of the deformation analysis. Then, additional advantages of the photogrammetry are discussed. Lastly, the difficulties which were encountered in the tests and difficulties which are expected when other quay walls are measured, are discussed.

5.1. Photogrammetric estimation quality

The main question to answer from the results is whether the quality of the deformation estimation is good enough to make photogrammetric deformation analysis a viable alternative to the tacheometric deformation analysis currently used. The results of the mock quay wall show that in near optimal conditions the photogrammetric deformation estimations are just as good as the tacheometric deformation estimation. The difference between the methods is sub-millimeter, which is within the precision of the tacheometry. This means the method of photogrammetric deformation analysis works.

A real quay wall does not have these optimal conditions, however even in a real quay wall test the photogrammetric deformation analysis shows very good results. From the estimated a posteriori standard deviation of a single epoch adjustment of the Schinkelkade, it is found that points on the wall reach a precision of 1.5 millimeter and below. Going further in the deformation analysis it is found that a hypothesis of no deformation is accepted and a conclusion can be made that the Schinkelkade is not significantly deforming. When an alternative deformation hypothesis is used to retrieve a deformation estimation, it is found that the Schinkelkade deformation estimation is maximum 3 millimeters. The Schinkelkade is assumed to be not deforming, so the result has a maximum error of 3 millimeters means that a 15 millimeter deformation is reliably detectable. This means the photogrammetric deformation analysis quality is good enough to be an quay wall monitoring alternative.

The deformation quality could be even better as proved in the mock wall test, where the difference between tacheometry and photogrammetry are within the standard deviation of the measurements. One difference between the mock wall and the real quay wall is the precision of the image point observations. The barcode detection at the mock wall is more precise than the SIFT feature detection at the Schinkelkade. This means the real quay wall with the SIFT observations has a higher a priori standard deviation. This influences the strength of the adjustment and the quality of statistical testing. There are two options to make the observations more precise: either use a different feature detection and matching algorithm or improve the observations achieved with SIFT.

Due to the time constraint only SIFT, SURF and ORB were investigated in the research for this thesis. Both SURF and ORB are feature detection algorithms similar to SIFT. SURF and ORB were mainly developed to improve the speed over SIFT. A real precision improvement will not come from SURF or ORB. SIFT, SURF and ORB are already older algorithm, more recently deep learning feature detec-

tors/matchers are developed. With these new algorithms an improvement in precision is possible.

The other way to improve precision is to improve the SIFT result. This is achieved by using a least-squares adjustment matching of the features in the images using the SIFT features as a approximation to improve. The least-squares matching makes an adjustment the feature point to be more precise, which will directly improve observation precision. It is expected that using least-squares will improve the standard deviation of the observations to at best $1/10$ pixel, where SIFT has a standard deviation of 1 to $1/2$ pixels.

Another improvement to the overall quality is made by having the reference plates with the control points closer together. The precision of the deformation estimations gets better when closer to the control points. For the Schinkelkade, it was chosen to put a reference plate with control points every 50 meters of quay wall. This 50 meter was a guess to what was needed to reach the required estimation quality. The required quality is reached with the 50 meter interval. However, a shorter interval could improve the deformation estimation significantly. The disadvantage of having the reference plates closer together is that more reference plates are required for the same length of quay wall and these reference plates have to be measured by tacheometer and that is time consuming. This would be a consideration the surveyor has to make.

5.2. Measurement & Computation time

The photogrammetric deformation estimation quality is as required, but this is not enough, there should also be a significant time improvement over the tacheometric deformation monitoring to be able to measure quay walls at a large scale. Photogrammetry is definitely a quicker measurement of the quay wall, where in the Schinkelkade test the photogrammetric method takes about a third of the time to measure the same length of quay wall compared to the tacheometric method. There are also still ways to further improve measurement speed, for example by using a multi-camera system that takes pictures at multiple orientations at once. In this way it would not be necessary to do multiple runs of making images along the quay wall, in a single run all images in different orientations can be made.

In processing, the photogrammetric method is slower than the tacheometric method. The photogrammetric deformation measurements need more processing to retrieve the final deformation estimations. The current tacheometric monitoring only requires an adjustment of every epoch after which the deformations are retrieved by simply calculating the difference between coordinates. The photogrammetric deformation analysis presented in this research needs multiple steps of processing including image feature detection and matching, single-epoch adjustment and a multi-epoch deformation adjustment from which the deformation estimations are retrieved. Especially the image feature matching is a time consuming process when many images are used. Also, the method of retrieving deformation from a deformation adjustment, as described in this research, is slower than simply subtracting coordinates. Photogrammetric deformation estimation can also be retrieved using the simply coordinate subtraction. And in the same way the tacheometric deformation estimation can also be retrieved using a deformation adjustment. The reason the deformation adjustment is used is that it gives advantages, namely different deformation equations can be integrated, stochastic observations are directly used in the deformation estimation and statistical testing is possible to test the quality of the adjustment and deformation hypothesis. This is a more time consuming process, but it will not impede the ability of the photogrammetry to be faster than tacheometry as the processing is automated and does not take manual work. The processing only requires the images and control points coordinates as input.

Furthermore, there are still improvements possible to the photogrammetric processing. For example, using image overlap estimations to only match features in images that overlap. Also, all processing is currently run on the central processing unit of the computer, however many of the processing steps can utilize the graphics processing unit to make the processing faster.

5.3. Coverage of deformation results

Next to the time cost, another big improvement of photogrammetric deformation analysis, compared to tacheometric deformation analysis, is the amount of deformation points on the quay wall. Where the

tacheometry retrieves a deformation point ever 5 to 10 meters, the photogrammetry retrieves a deformation estimation at approximately 300 points/m^2 of quay wall. This massive measurement density improvement gives us possibilities to improve the presentation and interpretation of the deformation.

Currently, the tacheometric deformation estimations are presented in 2D plots with a separate plot for the deformation in every direction. An example of such a plot with the deformation in Y direction is shown in Figure 5.1. Figure 5.1 is essentially the same plot as the Y deformation plot in Figure 4.14. These plots are good for visualising deformations even if the scale of those deformations are small. However, this visualization removes the advantage of the photogrammetric deformation analysis that deformations over the whole wall are measured. This visualization squeezes the entire height of the wall to a line. This means that if the top of the wall is deforming differently from the bottom of the wall this would not be seen in this plot even though it is detectable from the photogrammetric deformation analysis. To be able to see the deformation over the whole wall a 3D point cloud is used, as seen in Figure 4.15. In this 3D view the deformation points are coloured to the deformation size in a certain direction. It is harder to see small deformation differences over the whole, but the deformation point distribution is nicely preserved and deformation trends over the whole wall are visible.

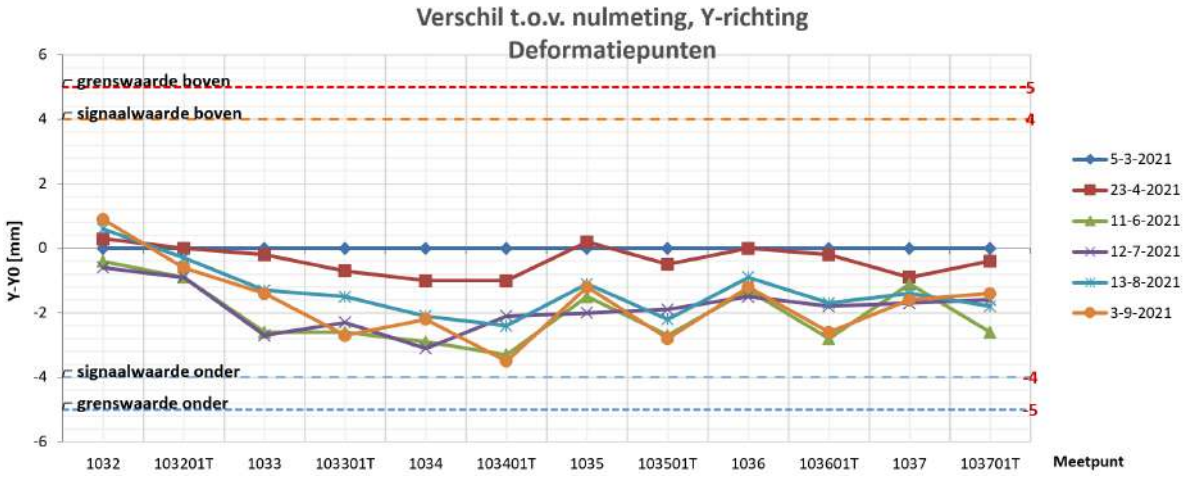

Figure 5.1: An Example of the currently used deformation visualization as made by the surveyor. It shows deformation estimations in Y-direction from 6 epochs retrieved from tacheometric deformation analsyis. The X-axis represents deformation points in order along the quay wall and the Y-axis the deformation size in Y-direction. Five epochs are measured and their deformation relative to the first epoch is presented. Two deformation thresholds are also shown in this figure. A signal threshold at 4 mm and boundary threshold at 5 mm. If there are deformations bigger than these thresholds they will be indicated in the deformation report.

5.4. Examining the deformation results

Another limitation in the current presentation of the deformation is a the ability to check the measurements and inspect possible deformations. When a tacheometric deformation analysis shows that there is a deformation, there is no possibility to further inspect this. The deformation estimation value is the only output the tacheometry gives. In this aspect the photogrammetric deformation analysis is also able to improve the deformation analysis presentation and subsequently the interpretation. The deformation points from photogrammetry can be projected into the images. In this way it is made visible where exactly on the wall the deformation occurs and additionally a visual inspection of that quay wall is immediately possible. If a deformation is found, it can be located in the images and it is possible to see if there are cracks or other indications of deformations. It is even possible to go through the images of multiple epochs and see cracks forming around suspected deformations. An example of projected deformation points in an image is shown in Figure 5.2.

Figure 5.2: Deformation point visualization where the deformation points are projected onto the images used in the deformation analsyis. In this image the deformation points are coloured to the deformation size in Y direction (into the quay wall).

5.5. Further possibilities with deformation results

As a by-product of the photogrammetric deformation analysis, a 3D point cloud of the wall is made. This point cloud can be used for a 3D visualizations, as is done in Figure 4.15. It is also possible to use this point cloud to make a 3D model of the quay wall, using for example a triangulation between the points to make a 3D mesh of the wall. This 3D mesh model of the quay wall can then be used to do finite-element analysis on the quay wall. This makes it possible to do more extensive modelling of failure of the quay wall and improve the understanding of the cause and effect of different failure mechanisms.

5.6. Application of the deformation analysis

The Schinkelkade quay wall is a fairly standard brick city quay wall. The Schinkelkade is representative for many kilometers of quay wall in not only Amsterdam, but also other cities such as Utrecht and The Hague. However, the Schinkelkade will not be representative for every quay wall. This means results of this research could not be representative for those different quay walls. And some of the choices made in measurement and processing could be incorrect for other quay walls.

The only problem encountered during the Schinkelkade measurements is obstruction of the view. If the quay wall is not visible no deformation points are found. This problem occurs when boats or vegetation are in front of the quay wall as the wall will not be visible then. Removal of obstruction is the only way to solve this problem. For boats this would require some preparation before measurements to notify boat owners to not moor to the quay wall. With houseboats this will be difficult as they can not easily move. The vegetation is not a big problem in winter as there is not much vegetation to block the view. In the other seasons the vegetation is an obstruction. Problematic vegetation should be moved out of the way or removed. Of course, it is also possible to accept that in that epoch a part of the quay wall does not have points. The deformation analysis will still work for the rest of the quay wall if the images at the obstruction have enough common points to make the system connected between subsequent reference plates.

A possible problem that could occur with other quay walls is a lack of texture on the quay wall. The feature point detection needs characterisable features in the images to work. For the photogrammetric deformation analysis the required amount of features is enough features to link all images together. With less features the adjustment will be weaker, however this can be compensated by moving the reference plates closer together. For the Schinkelkade, a 50 meter interval between reference plates

was enough to reach good deformation estimation quality. In general, brick quay walls and basalt quay walls (Figure 5.3a) will have enough features, but untextured concrete quay walls (Figure 5.3b) or sheet pile walls will not have enough reliably identifiable features. This can be solved by adding textures to these quay wall. For example, putting paint sprinkles on the will which will make for great identifiable features.

(a) Basalt quay wall, which has a good texture for finding features.

(b) Concrete quay wall, which has a bad texture for finding features.

Figure 5.3: Quay walls from different materials.

The features found have to be matched between the epochs. To make this possible features need to be similar in the epochs. This means the quay wall should look the same throughout the measurements. For example, when a quay wall is completely painted between epochs, the matching between the pre-painted features and post painted features will be hard. And the amount of deformation points will be heavily reduced.

The photogrammetric deformation analysis is only tested on quay walls, however the only assumption made specific to a quay wall is that only points of the quay wall are taken as deformation points. This means that the deformation analysis is possible on any object as long as you can take pictures with detectable features and there are reference points in the images. As this is untested it is unclear what the quality of the estimated deformation will.

5.7. Deformation outliers

In a closer look upon the deformation points, it is seen that there are outliers with much higher deformations than the deformation points around it. Using the photogrammetric advantage of being able to inspect the observations plotted in the image, like shown in Figure 4.13, it is found that these outliers can be contributed to incorrect feature matches. An example of this can be seen in Figure 5.4, here 3 image observation of a feature are shown. These three observations include a correct match, an incorrect match with a close feature and a vastly incorrect match.

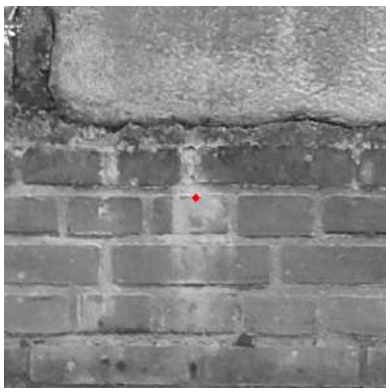

(a) Feature ”277585” in image ”2638” in epoch 4, correct feature.

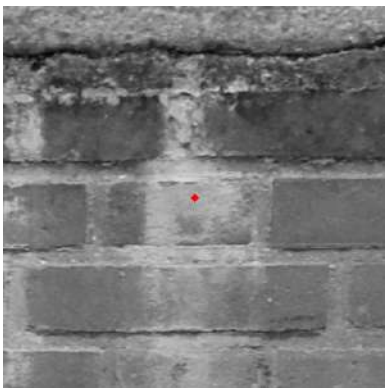

(b) Feature ”277585” in image ”0929” in epoch 3, incorrectly positioned feature.

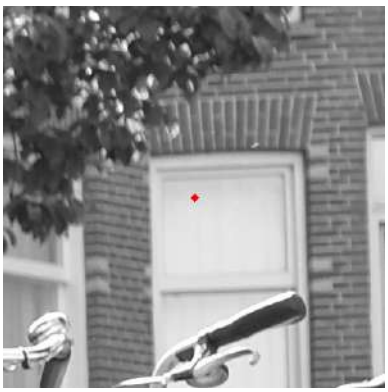

(c) Feature ”277585” in image ”2118” in epoch 4, incorrectly matched feature.

Figure 5.4: Example of errors in feature matching. Three matches of feature ”277585” is are shown, where one is correct and the other two are incorrect.

This mismatching problem is currently not detectable by the w-test, because every deformation parameter only has one observation. In the future, this can be solved by using more complex deformation equations which use more deformation observations per deformation parameter. However, these matching blunders do not seem to be a problem as there are much more correctly matched points around the blunders so they are easily distinguished. As is shown in Figure 5.2: there are points on the quay wall with a incorrect high deformation, however around those points are many more correct points with low deformation. Extra strict feature matching could also reduce the outliers, however this would remove many good points, which could be harmful to the deformation adjustment. The easiest way to remove the outliers is through the visualization. Instead of showing every deformation point, the deformation in the quay wall is interpolated and the interpolated deformation is shown. For example by rasterizing the quay wall and calculating the mean or meadian deformation in every cell.

5.8. Rotation estimation problem

During the wooden mock wall test, described in subsection 4.1.1, it is found that when rotation of the coordinate transformation is estimated in the adjustment, the convergence of the system is slow. A possible cause of this convergence problem is that all observed points are close to being in a plane. This is a bad geometry for estimating the rotations. A possible solution to this handling the adjustment differently, for example using the B-model in the adjustment. This problem did not hinder the tests, as the deformation estimation is not affected by this and it was possible to put the references in the same coordinate system for every epoch. It would be better if convergence is good when estimating the rotations, because it would not mess up the statistical testing of the transformation observations and parameters.

6

Conclusion

Failure of quay walls is a big problem in cities as Amsterdam. To solve this problem a lot of renovation is needed. To minimize dangerous situations, prioritization of the most unstable quay walls is needed. Quay wall failure is found to be often predictable by deformations in the wall. Currently, quay wall deformation measurements are only done by tacheometry, however this method is too slow for the scale of the problem. A innovative deformation monitoring method is needed. What are the requirements from the organisations involved?

- A 15 mm deforming quay wall must be reliably detected.
- Measurements must be faster than the current tacheometric method.

Photogrammetric deformation analysis is proposed in this research as a solution. What quality of deformation is possible?

- A similar deformation precision (0.5 mm) to tacheometry in optimal conditions is possible.
- A deformation precision of 3 mm on a quay wall is possible in practice.
- A measurement time 3 times quicker than by tacheometer

Is this quality good enough? This quality fulfils the requirements set for the new deformation method. The photogrammetric deformation analysis is capable of retrieving precise deformation estimations of a quay wall with a fast measurement time. Additional benefits of using the photogrammetric deformation analysis over tacheometry are:

- A higher measurement point density on the quay wall.
- Statistically tested results.
- 3D deformation visualization.
- Ability to perform visual inspection.

What is the data acquisition work flow of the photogrammetric deformation analysis and how to form observations from the photogrammetric measurements? First, reference plates are placed on the quay wall and measured in by tacheometer. Images are taken of the whole quay from a boat at different orientation to the quay wall. In the images of the quay wall, observations are retrieved of points visible in multiple images, using a computer vision feature point detection and matching algorithm. Using these image points and the reference plate points, the images and points are placed in 3D space and adjusted using bundle block adjustment. Then, this imaging is repeated with some months interval. With multiple measurements of the same quay wall, deformation analysis process can begin.

How to build the non-linear least squares adjustment for deformation analysis? Deformation points (points present in multiple epochs) are found using feature matching. The deformation analysis is done using a non-linear adjustment based on Velsink [34], which integrates the measurements of all epochs and estimations of coordinate transformations between epochs and deformations between epochs. This makes the deformation analysis independent of the coordinate system and the deformation is directly retrieved from the observations, which means the stochastic nature of the observation is taken into account. The coordinate transformation and deformation are added to the adjustment by non-stochastic observations. Coordinate transformation uses a similarity transformation as observation

equation and the deformation equation is defined by the deformation hypothesis. From this adjustment the deformation estimations are retrieved.

How to test the adjustment to find the best hypothesis? After multiple deformation adjustments using different deformation hypothesis are performed, the results are tested by an Overall Model Test. The Overall Model Test of all adjustments are compared to each other using the test ratio and the best deformation adjustment is chosen. From this deformation adjustment the deformation estimation for every deformation point is retrieved.

Finally, to what extend is it possible to do stochastic least-squares adjustment based deformation analysis on a quay wall using photogrammetry? The photogrammetric deformation analysis is a capable deformation monitoring method to be used as an faster alternative to tacheometric deformation monitoring. The precision is high enough to reliably detect unstable quay walls and additional advantages of photogrammetry and multi-epoch deformation adjustment, such as the deformation in 3D over the whole quay wall, statistically tested results and possibility for visual inspection, improve upon the tacheometric deformation method. The photogrammetric deformation analysis cannot be used when the quay walls are visually obstructed or textureless. On such quay walls the tacheometry will still be needed. However, excluding these quay walls there are still many kilometers of quay wall where photogrammetric deformation analysis can be used.

6.1. Recommendations

For future work on the photogrammetric deformation analysis, it would be most useful to expand the possible deformation hypotheses. In this thesis two hypotheses developed and they were not using any temporal and spatial relations between points, which could make the adjustment better. Also, the feature detection and matching algorithms have a big influence on the total process. There are many more modern alternative algorithms, which could be exploited for this photogrammetric deformation analysis. For example, the SuperGlue algorithm [29], which uses a neural network to match image features. Finally, the photogrammetric deformation analysis is developed and tested for application on a quay wall. However, the method of this research should also be applicable to other deforming systems. It would be interesting for future work to investigate this method on different deforming systems.

A

Closed form backwards intersection

In this appendix, a new closed-form backwards intersection algorithm is explained. The goal of the backward intersection is to determine the exterior parameters (position and orientation) of an image from the observations of known points in the image. It is partially based on a method proposed by Zeng and Wang [36] with a trilateration (3D position determined from three distances to known points) based on Askari and Barekat [1]. As input there are 4 known points denoted by A, B, C and D. All known points have known terrain coordinates X_k, Y_k, Z_k and known image coordinates x_k and y_k, where k is A, B, C or D. Also the focal distance f of the image is known. In the first part of the backward intersection point D will not be used. Point D is used later to reduce the possible answers to one.

A.1. Radii from geometry

The first step is to calculate the distances between the camera T position and three of the known points (A, B and C) in the image. This is a geometric problem where using the distances between points in 3D and distances between points in the image are used. It also involves solving a quartic equation. The complete derivation of the quartic equation can be found in Zeng and Wang [36]. A quartic equation has four roots. Of those four roots only the roots without an imaginary part are used. From every real root n a set of radii is calculated. This is the distance between camera T and the three known points A, B and C denoted as R_A, R_B and R_C. These radius equations are defined by Zeng and Wang [36]. For R_B there are 4 ways to calculate it. However there is only one right answer, which is the answer that results from 2 of the equations.

$$R_A = \frac{D_{CA}}{\sqrt{n - Q_{CA} * n + 1}} \tag{A.1}$$

$$R_C = n * R_A \tag{A.2}$$

$$R_{B(1)} = \frac{Q_{AB} * R_1 + \sqrt{Q_{AB}^2 * R_1^2 - 4 * R_1^2 - D_{AB}^2}}{2} \tag{A.3}$$

$$R_{B(2)} = \frac{Q_{AB} * R_1 - \sqrt{Q_{AB}^2 * R_1^2 - 4 * R_1^2 - D_{AB}^2}}{2} \tag{A.4}$$

$$R_{B(3)} = \frac{Q_{BC} * R_3 + \sqrt{Q_{BC}^2 * R_3^2 - 4 * R_3^2 - D_{BC}^2}}{2} \tag{A.5}$$

$$R_{B(4)} = \frac{Q_{BC} * R_3 - \sqrt{Q_{BC}^2 * R_3^2 - 4 * R_3^2 - D_{BC}^2}}{2} \tag{A.6}$$

where:

$$D_{AB} = \sqrt{(X_A - X_B^2) + (Y_A - Y_B^2) + (Z_A - Z_B^2)} \tag{A.7}$$

$$D_{BC} = \sqrt{(X_B - X_C^2) + (Y_B - Y_C^2) + (Z_B - Z_C^2)} \tag{A.8}$$

$$D_{CA} = \sqrt{(X_C - X_A^2) + (Y_C - Y_A^2) + (Z_C - Z_A^2)} \tag{A.9}$$

$$Q_{AB} = \frac{(2x_a x_b + 2y_a y_b + 2f^2)/f^2}{\sqrt{(x_a^2 + y_a^2 + f^2)(x_b^2 + y_b^2 + f^2)/f^2}} \tag{A.10}$$

$$Q_{BC} = \frac{(2x_b x_c + 2y_b y_c + 2f^2)/f^2}{\sqrt{(x_b^2 + y_b^2 + f^2)(x_c^2 + y_c^2 + f^2)/f^2}} \tag{A.11}$$

$$Q_{CA} = \frac{(2x_c x_a + 2y_c y_a + 2f^2)/f^2}{\sqrt{(x_c^2 + y_c^2 + f^2)(x_a^2 + y_a^2 + f^2)/f^2}} \tag{A.12}$$

As there are maximum four roots, there are possibly four sets of radii R_A, R_B and R_C. The next part of the closed-resection should be done with all radii-sets. Later, possible solutions will be eliminated.

A.2. Position by trilateration

From the radii-set the position of the camera is calculated using trilateration. Trilateration is the calculation of a position from distances to known points. Trilateration is the principle on which, for example, GPS position is determined using the distances to known satellite positions. The trilateration algorithm used is based on Askari and Barekat [1]. This algorithm solves general trilateration by translation and rotation to a non-general situation where trilateration is easier to solve. This is the situation where the three points (P_1, P_2 and P_3) in the trilateration are in the form of Equation A.13:

$$P_1 = \begin{bmatrix}0\\0\\0\end{bmatrix},\ P_2 = \begin{bmatrix}x_2\\0\\0\end{bmatrix},\ P_3 = \begin{bmatrix}x_3\\y_3\\0\end{bmatrix} \tag{A.13}$$

To get the known points A, B and C, they have to be made in the form of Equation A.13. First they are put in vectors and these vectors are translated by $-A$ too center the points on point A and put $\vec{A}$ in the form of P_1 of Equation A.13.

$$A = \begin{bmatrix}X_A\\Y_A\\Z_A\end{bmatrix} - \begin{bmatrix}X_A\\Y_A\\Z_A\end{bmatrix} = \begin{bmatrix}0\\0\\0\end{bmatrix},\ B = \begin{bmatrix}X_B\\Y_B\\Z_B\end{bmatrix} - \begin{bmatrix}X_A\\Y_A\\Z_A\end{bmatrix} = \begin{bmatrix}X_B - X_A\\Y_B - Y_A\\Z_B - Z_A\end{bmatrix},\ C = \begin{bmatrix}X_C\\Y_C\\Z_C\end{bmatrix} - \begin{bmatrix}X_A\\Y_A\\Z_A\end{bmatrix} = \begin{bmatrix}X_C - X_A\\Y_C - Y_A\\Z_C - Z_A\end{bmatrix} \tag{A.14}$$

Then, the xy-plane needs to coincide with the plane through points A, B and C, denoted by plane ABC. This means the perpendicular vector N to the plane ABC needs to coincides with the z-axis.

The rotations are determined from the vector N perpendicular to plane ABC. As $\vec{A}$ is a zero vector, the calculation of N is simply the cross-product between $\vec{B}$ and $\vec{C}$. Only direction of N is needed, so N is normalized.

$$\hat{N} = \frac{\vec{B} \times \vec{C}}{|N|} \tag{A.15}$$

Given $\hat{N}$, the rotations to make it coincide with the z-axis are calculated. There are two rotations necessary. Rotations are used in the form of rotation matrices where an angle is the input. However, from the geometry of the situation, $\cos\theta$ and $\sin\theta$ can be calculated directly from $\hat{N}$. There is no need to calculate the angle itself. These $\cos\theta$ and $\sin\theta$ calculation are found in Askari and Barekat [1]. This

gives rotation matrix $R_Z(\theta)$ defined in Equation A.16, which is a rotation around the z-axis rotating the $\hat{N}$ onto the xz-plane.

$$R_Z(\theta) = \begin{bmatrix} \cos\theta & \sin\theta & 0 \\ -\sin\theta & \cos\theta & 0 \\ 0 & 0 & 1 \end{bmatrix} \tag{A.16}$$

After $\hat{N}$ is rotated onto the xz-plane with $R_Z(\theta)$, the rotation $R_Y(\psi)$, defined in Equation A.17, is used to rotate $\hat{N}$ onto the z-axis. As with $R_Z(\theta)$ the $\cos\psi$ and $\sin\psi$ are calculated using geometry from $\hat{N}$ [1].

$$R_Y(\psi) = \begin{bmatrix} \cos\psi & 0 & -\sin\psi \\ 0 & 1 & 0 \\ \sin\psi & 0 & \cos\psi \end{bmatrix} \tag{A.17}$$

Rotations $R_Z(\theta)$and $R_Y(\psi)$ are applied on the coordinate vectors. The order of rotating is important as we later need to reverse the rotations.

$$\overrightarrow{A_{xy}} = (R_Z(\theta) * \vec{A}) * R_y(\psi) \tag{A.18}$$

$$\overrightarrow{B_{xy}} = (R_Z(\theta) * \vec{B}) * R_y(\psi) \tag{A.19}$$

$$\overrightarrow{C_{xy}} = (R_Z(\theta) * \vec{C}) * R_y(\psi) \tag{A.20}$$

With these rotation the z value of vectors $\overrightarrow{A_{xy}}$, $\overrightarrow{B_{xy}}$ and $\overrightarrow{C_{xy}}$ are set to zero. Now, to put the y value of $\overrightarrow{B_{xy}}$ to zero an additional rotation is needed. This is done with a rotation around the z-axis, using rotation matrix $R_Z(\phi)$, which rotates the vector $\overrightarrow{B_{xy}}$ to coincide with the x-axis. The $\cos\phi$ and $\sin\phi$ are calculated using geometry from $\overrightarrow{B_{xy}}$ [1].

$$R_Z(\phi) = \begin{bmatrix} \cos\phi & \sin\phi & 0 \\ -\sin\phi & \cos\phi & 0 \\ 0 & 0 & 1 \end{bmatrix} \tag{A.21}$$

Applying the rotation to $\overrightarrow{A_{xy}}$, $\overrightarrow{B_{xy}}$ and $\overrightarrow{C_{xy}}$.

$$\overrightarrow{A_x} = R_Z * \overrightarrow{A_{xy}}$$
$$\overrightarrow{B_x} = R_Z * \overrightarrow{B_{xy}}$$
$$\overrightarrow{C_x} = R_Z * \overrightarrow{C_{xy}}$$

With the rotation, $\overrightarrow{A_x}$, $\overrightarrow{B_x}$ and $\overrightarrow{C_x}$ are written in the form.

$$\overrightarrow{A_x} = \begin{bmatrix} 0 \\ 0 \\ 0 \end{bmatrix},\ \overrightarrow{B_x} = \begin{bmatrix} x_2 \\ 0 \\ 0 \end{bmatrix},\ \overrightarrow{C_x} = \begin{bmatrix} x_3 \\ y_3 \\ 0 \end{bmatrix} \tag{A.22}$$

This allows us to do a simpler trilateration calculation, where the coordinates of camera in the translated and rotated system T'_X, T'_Y and T'_Z are calculated.

$$T'_X = \frac{R_1^2 - R_2^2 + x_2^2}{2x_2} \tag{A.23}$$

$$T'_Y = \frac{R_1^2 - R_3^2 + x_3^2 + y_3^2 - \frac{x_3(R_1^2 - R_2^2 + x_2^2)}{x_2}}{2y_3} \tag{A.24}$$

For T'_Z there are 2 possible answers, because three overlapping spheres have 2 intersection points in 3D space. These intersection points are mirrored with respect to the plane through the center of the three spheres. Because of the translation and rotations, the centres of the spheres are on the xy-plane, which means the T'_Z can have a positive or negative sign.

$$T'_{+Z} = \sqrt{R_1^2 - {T'_x}^2 - {T'_y}^2} \tag{A.25}$$

$$T'_{-Z} = -\sqrt{R_1^2 - {T'_x}^2 - {T'_y}^2} \tag{A.26}$$

This leaves the results.

$$T'_+ = \begin{bmatrix} T'_X \\ T'_Y \\ T'_{+Z} \end{bmatrix},\ T'_- = \begin{bmatrix} T'_X \\ T'_Y \\ T'_{-Z} \end{bmatrix} \tag{A.27}$$

The T'_+ and T'_- are in the rotated and translated coordinate system made to do this simpler trilateration. To put the results back in the original coordinate system of the terrain points the rotation and translation operations are reversed. The following operations were executed, a translation by $-\vec{A}$, a rotation by $R_Z(\theta)$, a rotation by $R_Y(\psi)$ and a rotation by $R_Z(\phi)$. In Equation A.28, A.29 and A.30 these operations can be seen as a single equation applied to $\vec{A}$, $\vec{B}$ and $\vec{C}$.

$$\vec{A_x} = R_Z(\phi) * (R_y(\psi) * (R_Z(\theta) * (\vec{A} - \vec{A}))) \tag{A.28}$$

$$\vec{B_x} = R_Z(\phi) * (R_y(\psi) * (R_Z(\theta) * (\vec{B} - \vec{A}))) \tag{A.29}$$

$$\vec{C_x} = R_Z(\phi) * (R_y(\psi) * (R_Z(\theta) * (\vec{C} - \vec{A}))) \tag{A.30}$$

For the reverse calculation of the results, the order is reversed and the translation is multiplied by -1 and the rotation matrices are inverted. In Equation A.31 and A.32 these reversed operations can be seen as a single equation applied to $\vec{T_+}$ and $\vec{T_-}$.

$$\vec{T_+} = R_Z(\theta)^{-1} * (R_y(\psi)^{-1} * (R_Z(\phi^{-1} * \vec{T'_+})) + \vec{A} \tag{A.31}$$

$$\vec{T_-} = R_Z(\theta)^{-1} * (R_y(\psi)^{-1} * (R_Z(\phi^{-1} * \vec{T'_-})) + \vec{A} \tag{A.32}$$

Notice that trilateration is done for every radii set and the result of the trilateration gives two answers. This makes that there are between 2 and 8 positions possible from the backward intersection calculations till now.

A.3. Orientation by bisection plane intersection

At this point the camera position T is known. The orientation has to be estimated to get the total exterior parameter set of the camera. The orientation is estimated using two of the known points and the camera position. In this orientation estimated a rotation axis and rotation angle is estimated in the form of a quaternion, Q.

$$Q = \begin{bmatrix} a \\ b \\ c \\ d \end{bmatrix} \tag{A.33}$$

The points A and B are chosen to be used to estimate the orientation. The vector from camera to the points in the terrain is estimated and normalized as angles between vectors is the only interest the normalization makes sure there is no scaling from the length of the vectors.

$$\hat{A_t} = \frac{\vec{A} - \vec{T}}{|A_t|}, \quad \hat{B_t} = \frac{\vec{B} - \vec{T}}{|A_t|} \tag{A.34}$$

Also the vector from camera to the point on the image is estimated and normalized. This vector is determined by the image point positions of the points (x_A, y_A, x_B and y_B) and focal length f of the camera.

$$\hat{a_t} = \frac{\begin{bmatrix} x_A & y_A & f \end{bmatrix}^T}{|a_t|}, \quad \hat{b_t} = \frac{\begin{bmatrix} x_B & y_B & f \end{bmatrix}^T}{|b_t|} \tag{A.35}$$

The orientation of the camera is equal to the rotation which rotates $\hat{a_t}$ onto $\hat{A_t}$ and $\hat{b_t}$ onto $\hat{B_t}$. First, the rotation axis g is found. The rotation axis is the vector of the intersection line between 2 planes. These planes are made from the bisection vectors between $\hat{a_t}$, $\hat{A_t}$ and $\hat{b_t}$, $\hat{B_t}$ and the vector perpendicular to

$\hat{a_t}$, $\hat{A_t}$ and $\hat{b_t}$, $\hat{B_t}$. The bisector vectors are named A_{bs} and B_{bs}, the perpendicular vectors are named A_p and B_p.

$$A_{bs} = |\hat{a_t}| * \hat{A_t} + |\hat{A_t}| * \hat{a_t}, \quad B_{bs} = |\hat{b_t}| * \hat{B_t} + |\hat{B_t}| * \hat{b_t} \tag{A.36}$$

$$A_p = \hat{a_t} \times \hat{A_t}, \quad B_p = \hat{b_t} \times \hat{B_t} \tag{A.37}$$

To get g, the intersection between the planes formed by A_p, A_{bs} and B_p, B_{bs} are estimated.

$$g = (A_p \times A_{bs}) \times (B_p \times B_{bs} = \begin{bmatrix} g_X \\ g_Y \\ g_Z \end{bmatrix} \tag{A.38}$$

The rotation around this rotation axis is also estimated.

$$\cos\gamma = \frac{(g \times \hat{A_t}) \cdot (g \times \hat{a_f})}{|(g \times \hat{A_t})| * |(g \times \hat{a_f})|} \tag{A.39}$$

From the rotation axis and rotation angle the orientation of the camera is estimated in the form of a quaternion.

$$Q_T = \begin{bmatrix} a \\ b \\ c \\ d \end{bmatrix} = \begin{bmatrix} \sqrt{\frac{1+\cos\gamma}{2}} \\ g_Y * \sqrt{\frac{1-a^2}{g_X^2+g_Y^2+g_Z^2}} \\ g_X * \sqrt{\frac{1-a^2}{g_X^2+g_Y^2+g_Z^2}} \\ g_Z * \sqrt{\frac{1-a^2}{g_X^2+g_Y^2+g_Z^2}} \end{bmatrix} \tag{A.40}$$

In other photogrammetric estimations the orientation of the camera is expected as a rotation matrix so an additional step is taken to make this translation.

$$R = \begin{bmatrix} d^2+a^2-b^2-c^2 & 2(ab+cd) & 2(ac-bd) \\ 2(ab-cd) & d^2-a^2+b^2-c^2 & 2(bc+ad) \\ 2(ac+bd) & 2(bc-ad) & d^2-a^2-b^2+c^2 \end{bmatrix} \tag{A.41}$$

As a result for every camera position, a orientation is estimated.

A.4. Answer selection by point projection

As a result from the previous steps, there are 2, 4, 6 or 8 possible exterior parameter sets for the camera. In this last step of the closed form resection, the right answer is found. This is done by using the projection error of the fourth known point D. The image coordinates (x_D, y_D) of a known point D can be calculated with the collinearity equations.

$$x_d = -f\frac{R_{11}(X_D - X_T) + R_{12}(Y_D - Y_T) + R_{13}(Z_D - Z_T)}{R_{31}(X_D - X_T) + R_{32}(Y_D - Y_T) + R_{33}(Z_D - Z_L)} \tag{A.42}$$

$$y_d = -f\frac{R_{21}(X_D - X_T) + R_{22}(Y_D - Y_T) + R_{23}(Z_D - Z_T)}{R_{31}(X_D - X_T) + R_{32}(Y_D - Y_T) + R_{33}(Z_D - Z_T)} \tag{A.43}$$

The terrain coordinates of D are known and there are multiple possible exterior parameters of the camera. For every possible camera exterior parameter set the image coordinates (x_d, y_d) of point D on the image are estimated. As the actual image coordinates of point D are also known (x_D, y_D) the error ϵ between estimated and actual image coordinates can be retrieved.

$$\epsilon = |\begin{bmatrix} x_d \\ y_d \end{bmatrix} - \begin{bmatrix} x_D \\ y_D \end{bmatrix}| \tag{A.44}$$

This error is zero for the correct set of exterior parameters if the known points are perfectly accurate. In practice, the exterior parameters are not perfectly accurate as there is measurement error in the known point coordinates and image point coordinates. So as a quality check the exterior parameters, which give the smallest projection error is chosen as result.

B

Mock quay wall test results

In this appendix, the deformation plots of the mock quay wall test are shown for every test in section B.1. Only the right wall is shown as the left wall is not deformed as control. Also the table with differences between the tacheometry and photogrammetry is displayed in section B.2 from this table Figure 4.4 is derived. In this table the exact differences between tacheometry and photogrammetry are shown.

B.1. Mock quay wall deformation plots

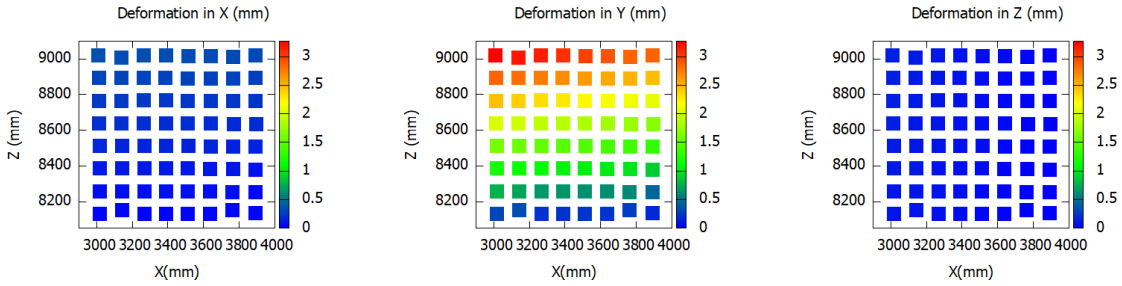

(a) Deformations of test 1

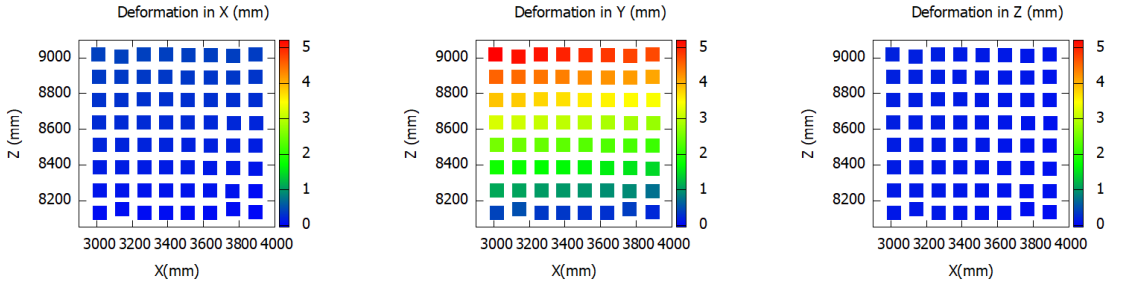

(b) Deformations of test 2

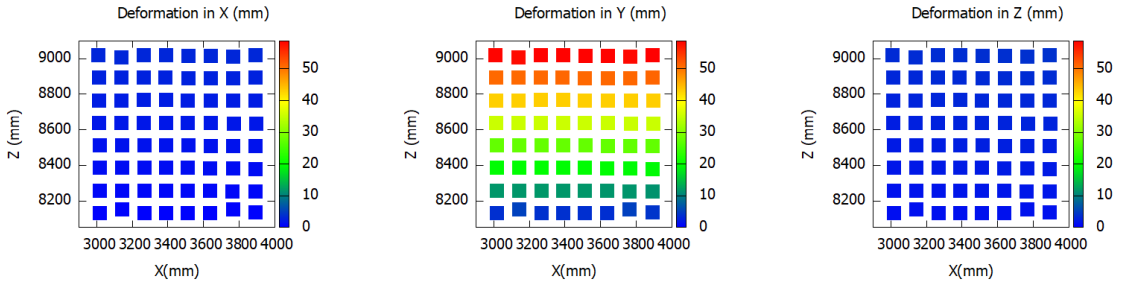

(c) Deformations of test 3

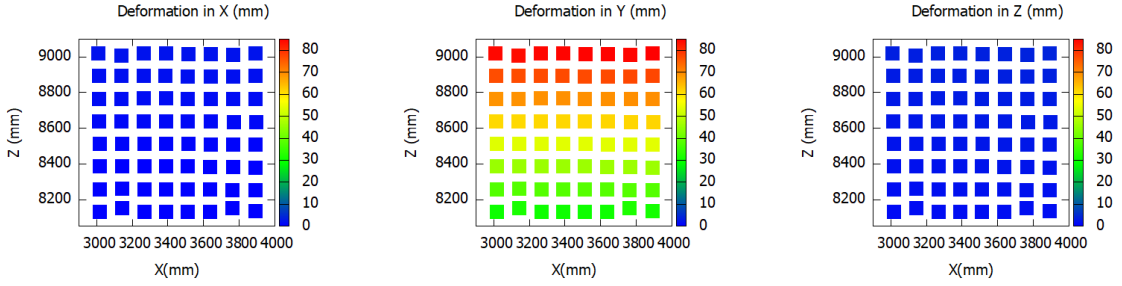

(d) Deformations of test 4

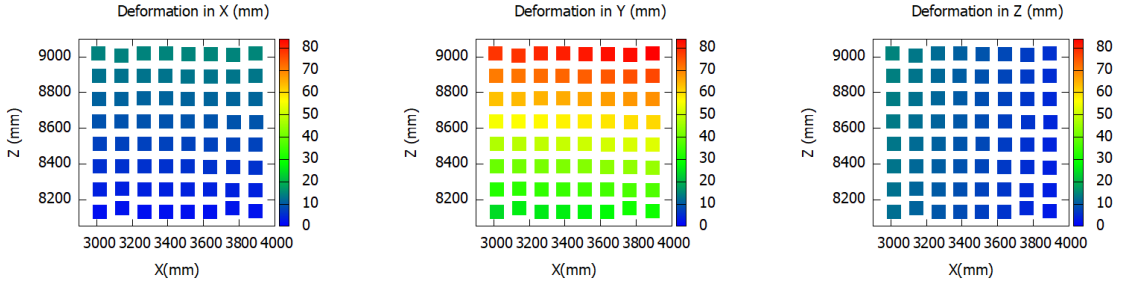

(e) Deformations of test 5

Figure B.1: 2D front view of the wooden mock quay wall, where the deformation points on the wall are coloured to the size of their deformation in a X, Y or Z direction for tests 1 to 5. The description of the deformations for every test are found in Table 4.1.

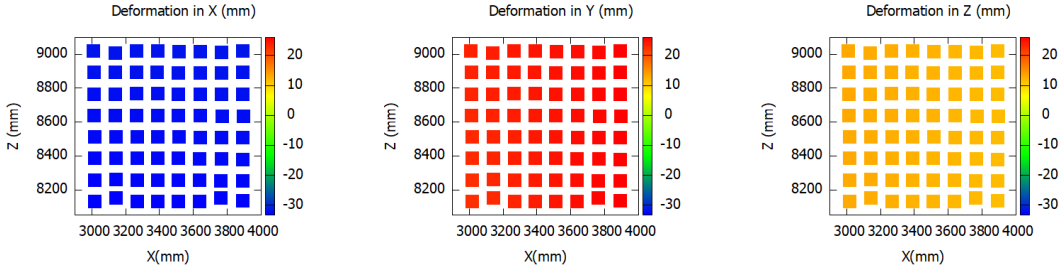

(a) Deformations of test 6

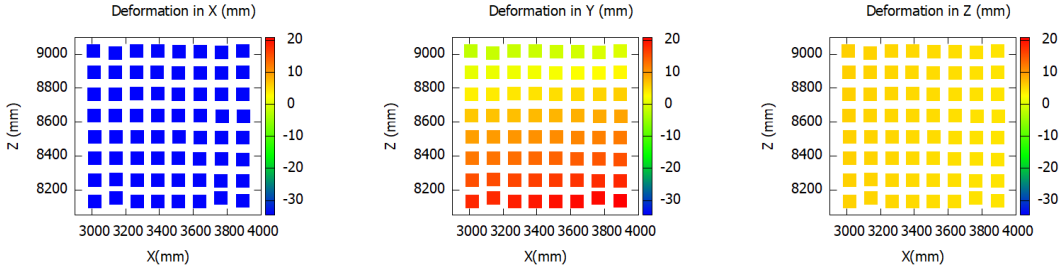

(b) Deformations of test 7

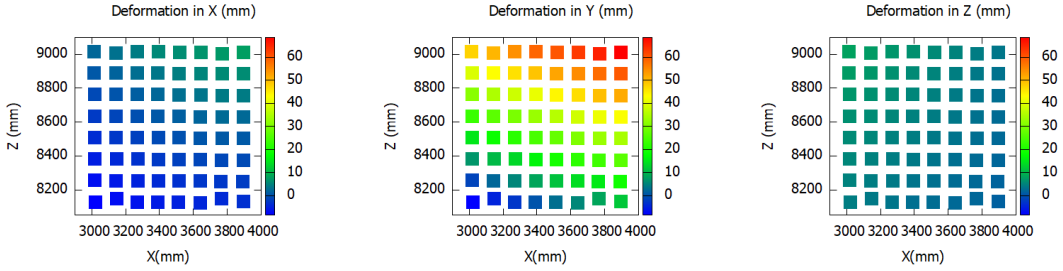

(c) Deformations of test 8

Figure B.2: 2D front view of the wooden mock quay wall, where the deformation points on the wall are coloured to the size of their deformation in a X, Y or Z direction for tests 6, 7 and 8. These tests were done with tilted plane deformation. The description of the deformations for every test are found in Table 4.1.

B.2. Tacheometry vs. Photogrammetry

		X-Deformation (mm)			Y-Deformation (mm)			Z-Deformation (mm)		
Test	Barcode	Tacheo.	Photo.	Diff.	Tacheo.	Photo.	Diff.	Tacheo.	Photo.	Diff.
1	Top Left	0.5	0.3	0.2	3.6	3.3	0.3	0.1	0.2	-0.1
1	Top Right	0.6	0.3	0.3	3.3	2.9	0.4	-0.1	0.1	-0.2
1	Bottom Left	0.3	0.0	0.3	0.9	0.4	0.5	-0.1	0.1	-0.2
1	Bottom Right	0.3	0.0	0.3	0.5	0.2	0.3	-0.2	0.0	-0.2
2	Top Left	0.5	0.4	0.1	6	5.2	0.8	0.1	0.2	-0.1
2	Top Right	0.4	0.3	0.1	4.8	4.6	0.2	-0.1	0.1	-0.2
2	Bottom Left	0.3	0.0	0.3	0.9	0.3	0.6	-0.1	0.1	-0.2
2	Bottom Right	0.3	-0.1	0.4	0.5	0.1	0.4	-0.1	0.1	-0.2
3	Top Left	3	2.9	0.1	58.8	58.5	0.3	3.2	3.2	0.0
3	Top Right	2.7	3.0	-0.3	58.6	58.8	-0.2	3.7	3.7	0.0
3	Bottom Left	0.2	0.1	0.1	3.7	3.6	0.1	1	1.0	0.0
3	Bottom Right	0	0.2	-0.2	3.7	4.0	-0.3	1.4	1.3	0.1
4	Top Left	2.2	2.0	0.2	84.6	84.2	0.4	3.2	3.3	-0.1
4	Top Right	2.2	2.0	0.2	85	85.1	-0.1	3.7	3.8	-0.1
4	Bottom Left	-0.6	-0.8	0.2	30.2	29.7	0.5	1.1	1.2	-0.1
4	Bottom Right	-0.6	-0.7	0.1	30.4	30.5	-0.1	1.5	1.5	0.0
5	Top Left	14.2	14.3	-0.1	78.1	78.2	-0.1	14.2	14.3	-0.1
5	Top Right	14.5	14.7	-0.2	83.6	83.9	-0.3	5.1	5.3	-0.2
5	Bottom Left	1.7	1.6	0.1	23.9	24.0	-0.1	11.9	12.0	-0.1
5	Bottom Right	1.9	2.0	-0.1	28.8	29.5	-0.7	2.8	2.8	0.0
6	Top Left	-31.7	-31.9	0.2	24.1	23.5	0.6	12.8	12.9	-0.1
6	Top Right	-32.1	-31.7	-0.4	25.1	25.9	-0.8	11.3	11.5	-0.2
6	Bottom Left	-33.2	-33.4	0.2	22.7	22.5	0.2	12.7	12.8	-0.1
6	Bottom Right	-33.1	-33.1	0.0	26	26.1	-0.1	11.3	11.5	-0.2
7	Top Left	-34.3	-34.4	0.1	-2.2	-2.2	0.0	5.7	5.8	-0.1
7	Top Right	-34.3	-34.3	0.0	-0.2	-0.2	0.0	4.3	4.4	-0.1
7	Bottom Left	-34.4	-34.6	0.2	18.3	18.0	0.3	5.6	5.7	-0.1
7	Bottom Right	-34.4	-34.4	0.0	20.5	20.9	-0.4	4.4	4.4	0.0
8	Top Left	-7.2	-7.3	0.1	88.9	88.8	0.1	15.6	15.7	-0.1
8	Top Right	-0.7	-0.8	0.1	155.8	156.2	-0.4	16	16.2	-0.2
8	Bottom Left	-14.7	-14.7	0.0	35.2	35.6	-0.4	13.7	13.7	0.0
8	Bottom Right	-8.3	-8.5	0.2	102	102.4	-0.4	13.9	13.9	0.0

Table B.1: Comparison between the tacheometric and photogrammetric deformation estimation of the same barcodes. These barcodes were located in the top right, top left, bottom right and bottom left corners of the right mock quay wall. The tacheometric (Tacheo) and photogrammetric (Photo) estimated deformations in X, Y and Z direction are listed in the table together with the difference between the estimated deformations (Diff).

Bibliography

[1] P. Askari and F. Barekat. Trilateration and bilateration in 3d and 2d space using active tags. 10 2017.

[2] J. Ayscough. *A short account of the eye and nature of vision..* A. Strahan, 1752.

[3] W. Baarda. A testing procedure for using geodetic networks. *Publication on Geodesy, New Series*, 2, 1968.

[4] H. Bay, T. Tuytelaars, and L. Van Gool. Surf: Speeded up robust features. In *European conference on computer vision*, pages 404–417. Springer, 2006.

[5] D.C. Brown. Close-range camera calibration, photogrammetric engineering. *Engineering and Remote Sensing*, 37(8):855–866, 1971.

[6] M. Calonder, V. Lepetit, C. Strecha, and F.P. Brief. Binary robust independent elementary features. In *Proceedings of the European Conference on Computer Vision*, pages 778–792, 2010.

[7] L. Chen, F. Rottensteiner, and C. Heipke. Feature detection and description for image matching: from hand-crafted design to deep learning. *Geo-spatial Information Science*, 24(1):58–74, 2021.

[8] H.M. de Heus, M.H.F. Martens, and H.M.E. Verhoef. Stability-analysis as part of the strategy for the analysis of the groningen gas field levellings. In *Proceedings of the Perelmutter workshop on dynamic deformation models, Haifa, Israel*, volume 29, 1994.

[9] K.G. Derpanis. Outline of the relationship between the difference-of-gaussian and laplacian-of-gaussian. *NYU Dept. of CS & Eng*, pages 1–3, 2006.

[10] J. Dijstelbloem, E. ten Hulsen, T. Hilgers, and team Bruggen en Kademuren. Actieplan bruggen en kademuren. 07 2019.

[11] J.G. Fryer and D.C. Brown. Lens distortion for close-range photogrammetry. *Photogrammetric engineering and remote sensing*, 52(1):51–58, 1986.

[12] Global Survey. Leica robotic total stations comparison chart. `https://globalsurvey.co.nz/surveying-gis-news/leica-robotic-total-stations-comparison-chart/`. Accessed: 2021-07-26.

[13] C.G. Harris, M. Stephens, et al. A combined corner and edge detector. In *Alvey vision conference*, volume 15, pages 10–5244. Citeseer, 1988.

[14] D. Imparato, P.J.G. Teunissen, and C.C.J.M. Tiberius. Minimal detectable and identifiable biases for quality control. *Survey review*, 51(367):289–299, 2019.

[15] Y. Ke and R. Sukthankar. Pca-sift: A more distinctive representation for local image descriptors. In *Proceedings of the 2004 IEEE Computer Society Conference on Computer Vision and Pattern Recognition, 2004. CVPR 2004.*, volume 2, pages II–II. IEEE, 2004.

[16] G. Klein and D. Murray. Improving the agility of keyframe-based slam. In *European conference on computer vision*, pages 802–815. Springer, 2008.

[17] M. Korff, R. Esposito, and M. Hemel. Bezwijken grimburgwal. Technical report, Delft University of Technology, 2021.

[18] K. Kraus. *Photogrammetry: geometry from images and laser scans*. de Gruyter, 2007.

[19] D.G. Lowe. Object recognition from local scale-invariant features. In *Proceedings of the seventh IEEE international conference on computer vision*, volume 2, pages 1150–1157. Ieee, 1999.

[20] D.G. Lowe. Distinctive image features from scale-invariant keypoints. *International journal of computer vision*, 60(2):91–110, 2004.

[21] T. Luhmann, C. Fraser, and H. Maas. Sensor modelling and camera calibration for close-range photogrammetry. *ISPRS Journal of Photogrammetry and Remote Sensing*, 115:37–46, 2016.

[22] A.P. Mahmoudzadeh and N. Kashou. Evaluation of interpolation effects on upsampling and accuracy of cost functions-based optimized automatic image registration. *International journal of biomedical imaging*, 2013:395915, 08 2013. doi: 10.1155/2013/395915.

[23] OpenCV. Feature detection and description. https://docs.opencv.org/4.5.2/db/d27/tutorial_py_table_of_contents_feature2d.html. Accessed: 2021-08-16.

[24] J. Polman and M.A. Salzmann. Handleiding voor de technische werkzaamheden van het kadaster. *Kadaster, Apeldoorn*, pages 61–236, 1996.

[25] A. Ranzijn, M. van der Beek, and M. Kruyswijk. Kade ingestort in centrum amsterdam, situatie 'stabiel'. *Het Parool*. URL https://www.parool.nl/amsterdam/kade-ingestort-in-centrum-amsterdam-situatie-stabiel~b2f44086/.

[26] E. Rosten and T. Drummond. Machine learning for high-speed corner detection. In *European conference on computer vision*, pages 430–443. Springer, 2006.

[27] A. Roubos, F. Jonker, D. Grotegoed, and SBRCURnet. *Binnenstedelijke kademuren*. SBRCURnet, Rotterdam, 2014.

[28] E. Rublee, V. Rabaud, K. Konolige, and G. Bradski. Orb: An efficient alternative to sift or surf. In *2011 International conference on computer vision*, pages 2564–2571. Ieee, 2011.

[29] P. Sarlin, D. DeTone, T. Malisiewicz, and A. Rabinovich. Superglue: Learning feature matching with graph neural networks. In *Proceedings of the IEEE/CVF Conference on Computer Vision and Pattern Recognition (CVPR)*, June 2020.

[30] B. Stam. Gevraagd: nieuwe monitoringtechnieken voor amsterdamse bruggen en kademuren. *Technische Weekblad*. URL https://www.technischweekblad.nl/artikelen/tech-achtergrond/gevraagd-nieuwe-monitoringtechnieken-voor-amsterdamse-bruggen-en-kademuren.

[31] P.J.G. Teunissen, D.J. Simons, and C.C.J.M Tiberius. *Probability and Observation Theory*. VSSD Delft, 2006.

[32] Trimble. Compare mechanical total stations. https://geospatial.trimble.com/portfolios/253/compare. Accessed: 2021-07-26.

[33] R.R. van Buuren. Binnenstedelijke kadeconstructies, bezwijkingsmachanismen en verplaatsingen. Technical report, CRUX, 2018.

[34] H. Velsink. *The Elements of Deformation Analysis: Blending Geodetic Observations and Deformation Hypotheses.* PhD thesis, Delft University of Technology, Netherlands, 2018.

[35] J. Wang, F. Shi, J. Zhang, and Y. Liu. A new calibration model of camera lens distortion. *Pattern recognition*, 41(2):607–615, 2008.

[36] Z. Zeng and X. Wang. A general solution of a closed-form space resection. *Photogrammetric Engineering and Remote Sensing*, 58:327–327, 1992.